INSTITUTE FOR NUCLEAR STUDY
UNIVERSITY OF TOKYO
Tanashi, Tokyo 188
Japan

INS — J — 185
November 1996

Systematic Measurement of the Spin-Polarization of the Cosmic-Ray Muons

Shun'ichi Mine

Systematic Measurement of the Spin-Polarization of the Cosmic-Ray Muons

Shun'ichi Mine

Graduate School
University of Tokyo
7-3-1 Hongo, Bunkyo-ku, Tokyo 113 Japan

Systematic Measurement of the Spin-Polarization of the Cosmic-Ray Muons

Shun'ichi Mine

Graduate School
University of Tokyo
7-3-1 Hongo, Bunkyo-ku, Tokyo 113 Japan

Abstract

We have measured the longitudinal polarization of cosmic-ray muons employing a detector calibrated with a polarized muon beam. The polarizations were found to be 0.227 ± 0.017 (*stat*) ± 0.070 (*syst*) and 0.327 ± 0.056 (*stat*) ± 0.072 (*syst*) at 1 GeV and 14 GeV, respectively. The results obtained here are new reliable values in this energy region.

The effect on the atmospheric neutrino flux due to the muon polarization was estimated. Even if the polarization is taken into account, the anomaly of the ratio of the atmospheric muon neutrino flux to the atmospheric electron neutrino flux observed by Kamiokande, IMB-3, and Soudan-2 detectors still remains.

Contents

Chapter 1

Introduction

1.1 Air shower

In space, many kinds of particles, mainly protons and nuclei, fly isotropically. These particles are generated by astrophysical objects such as the shockwave of a supernova remnant, a pulsar, and are called primary cosmic-rays. Such primary cosmic-rays produce baryons or mesons via the hadronic interaction when they interact with the atmosphere of the earth. These produced particles are called secondary cosmic-rays. Light mesons such as pions or kaons are abundantly produced as secondary cosmic-rays. These light mesons decay or interact with the atmospheric nuclei before reaching the surface of the earth because the depth of the atmosphere (~ 1000 g/cm^2) corresponds to a length about ten times larger than the mean free path of the nuclear interaction [1].

The decay modes of the pion and the kaon are summarized in Table 1.1 [2]. A charged pion decays to a muon and a neutrino with nearly 100% branching-ratio. A neutral pion decays into two photons with almost 100% branching-ratio. An energetic photon converts to an electron-positron pair and makes an electromagnetic shower. The decay mode of the kaon is more complicated than that of the pion. However, the main decay mode of the charged kaon ($K \rightarrow \mu\nu$) is similar to that of the charged pion. Muons are finally generated directly or via the charged pion in most of the kaon decay modes.

The life time of an energetic cosmic-ray muon with an energy of about 1 GeV is approximately equal to the time needed to reach the surface of the earth. Some muons decay before they reach the surface of the earth and produce one electron (when the word 'electron' is used, it includes 'positron' as well in this paper) and two neutrinos. Since neutrinos are neutral particles, interact only via the weak force, and are thought to be stable within the standard model of particle physics, they reach the surface of the earth without any interactions and are called atmospheric neutrinos.

Repeating these successive interactions and decays of the particles, one primary cosmic-ray develops an extensive particle cascade called an extensive air shower. A schematic view of the air shower is shown in Figure 1.1.

A typical sea-level vertical flux for charged particles is 1.1×10^2 m^{-2}s^{-1}sr^{-1}. Approximately 75% of all particles at sea-level are muons and the rest are electrons. The fraction of protons is about 3.5% at 1 GeV, decreasing to about 0.5% at 10 GeV [2].

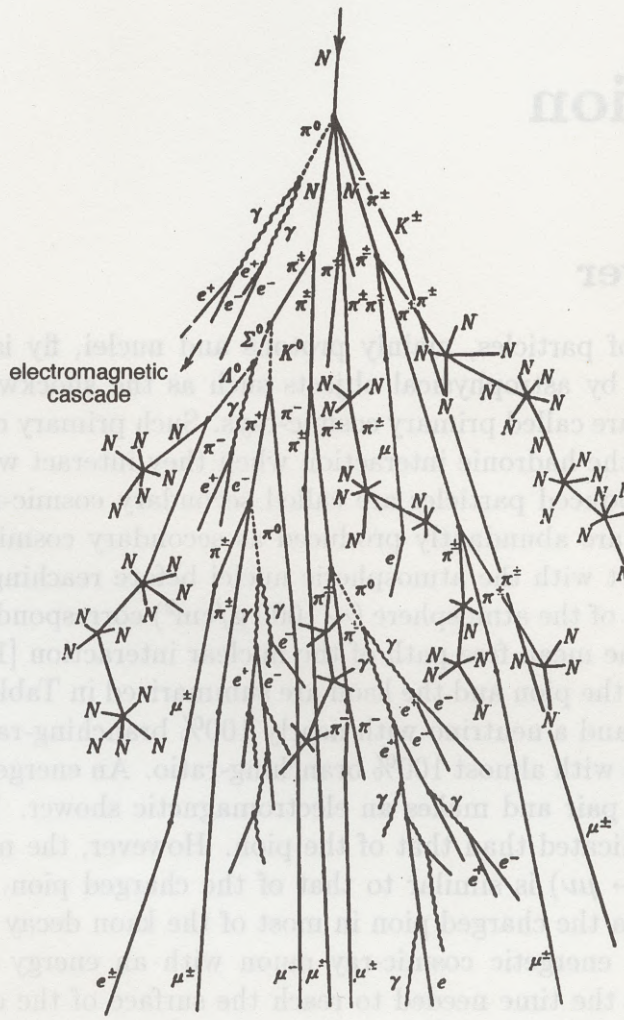

Figure 1.1: Schematic view of the air shower [1]. A primary cosmic-ray (N at top) develops an extensive particle cascade.

	Mode	Branching-ratio (%)
π^+	$\mu^+\nu_\mu$	99.99
π^0	2γ	98.80
	$e^+e^-\gamma$	1.20
K^+	$\mu^+\nu_\mu$	63.51
	$\pi^+\pi^0$	21.16
	$\pi^+\pi^+\pi^-$	5.59
	$\pi^0 e^+\nu_e$	4.82
	$\pi^0\mu^+\nu_\mu$	3.18
	$\pi^+\pi^0\pi^0$	1.73
K^0_S	$\pi^+\pi^-$	68.61
	$\pi^0\pi^0$	31.39
K^0_L	$\pi^\pm e^\mp\nu$	38.7
	$\pi^\pm\mu^\mp\nu$	27.0
	$3\pi^0$	21.6
	$\pi^+\pi^-\pi^0$	12.4
	$\pi^\pm e^\mp\nu_e\gamma$	1.3

Table 1.1: Summary of decay modes of the pion and kaon. Only the decay modes whose branching-ratio are greater than 1% are listed. The decay modes of negative mesons are charge conjugates of the above modes.

The muons at sea-level have a mean energy of 2 GeV and a differential spectrum falling as $\sim E^{-2}$, becoming $\sim E^{-3.6}$ above a few TeV. The angular distribution is $\sim\cos^2\alpha$, changing to $\sec(\alpha)$ at energies above one TeV, where α is the zenith angle at production [2].

1.2 Derivation of spin-polarization of cosmic-ray muons

The spin-polarization of cosmic-ray muons was calculated under the assumption that the interaction between the light mesons produced in the secondary interaction and the atmospheric nuclei was ignored and only the two-body decay of the light meson was considered [3].

The origin of the polarization of cosmic-ray muons can be understood in the following way. In the rest frame of the parent meson, the $\mu^\pm$ is fully polarized with a helicity ∓ 1 as shown in Figure 1.2. In the laboratory frame, however, the polarization is not complete because muons produced in the backward direction in the rest frame of the mesons may be Lorentz transformed into those moving forward. Here the direction of the muon momentum is reversed but the polarization is maintained to conserve the angular momentum of the system. If the velocity of the meson is larger than that of the decay muon in the rest frame of the meson, the decay muon moves forward in the laboratory frame.

The energy spectrum of the mesons is not flat but has a steep slope, decreasing

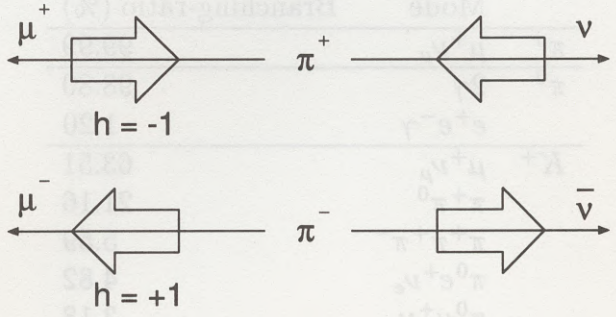

Figure 1.2: Schematic view of the decay of the charged pion at rest. The helicity of the decay product is shown by the open arrow.

with increasing energy. Consequently, the muons of a given energy are produced both forwardly from mesons of lower energies and backwardly from those of higher energies, and the intensity of the former mesons is greater than that of the latter.

Transforming along the momentum direction of the parent mesons, the component of the polarization along the momentum direction of the $\mu^{\pm}$ in the laboratory frame is given as (Appendix A):

$$P(E) = \mp\left(\frac{E_\mu E_\mu^*}{p_\mu p_\mu^*} - \frac{E}{M}\cdot\frac{m_\mu^2}{p_\mu p_\mu^*}\right), \tag{1.1}$$

where E (M) is the energy (mass) of the parent meson, E_μ (p_μ) is the energy (momentum) of the muon in the laboratory frame, m_μ ($\sim$106 MeV) is the mass of the muon, and E_μ^* (p_μ^*) is the energy (momentum) of the muon in the rest frame of the parent meson:

$$\begin{aligned} E_\mu^* &= \frac{M^2+m_\mu^2}{2M}, \\ p_\mu^* &= \frac{M^2-m_\mu^2}{2M} \end{aligned} \tag{1.2}$$

Substituting the mass of the parent meson in Eq.(1.2), E_μ^* (p_μ^*) becomes 110 (30) MeV and 258 (236) MeV for pion and kaon, respectively.

If the energy of the muon is fixed in the laboratory frame, the energy of the parent meson is limited between E_{max} and E_{min} defined as:

$$\begin{aligned} E_{max} &= \left(\frac{M}{m_\mu}\right)^2 E_\mu, \\ E_{min} &= E_\mu \end{aligned} \tag{1.3}$$

Evidently, the polarization of μ^+ (μ^-) is completely parallel (antiparallel) for $E = E_{max}$ and completely antiparallel (parallel) for $E = E_{min}$ to the muon direction. Substituting the mass of the meson in Eq.(1.3), E_{max} becomes $1.74\times E_\mu$ for pion and $21.83\times E_\mu$ for kaon.

The energy spectrum of the parent mesons at production was experimentally determined to be:

$$N(E) \equiv \frac{dN}{dE} = N_0 \cdot E^{-\alpha}, \tag{1.4}$$

where N_0 is a normalization constant, E is the energy of the meson, and α is about 2.65 above 6 GeV, and falls smoothly at lower energies [4].

Averaging Eq.(1.1) by weighting with Eq.(1.4), the polarization of the cosmic-ray muon at production is:

$$\begin{aligned} P_\mu &= \int_{E_{min}}^{E_{max}} P(E) \cdot N(E) \frac{dE}{E} \Big/ \int_{E_{min}}^{E_{max}} N(E) \frac{dE}{E}, \\ &= \frac{E_\mu E_\mu^*}{p_\mu p_\mu^*} - \frac{m_\mu^2}{M p_\mu p_\mu^*} \cdot \frac{\alpha}{\alpha - 1} \cdot \frac{E_{min}^{-(\alpha-1)} - E_{max}^{-(\alpha-1)}}{E_{min}^{-\alpha} - E_{max}^{-\alpha}}, \end{aligned} \tag{1.5}$$

where a factor $1/E$ in the upper equation is included to take into account the decay probability of the parent mesons and $0<\alpha<\infty$. Substituting α=2.65, E_μ^*=110 (258) MeV, and p_μ^*=30 (236) MeV in Eq.(1.5), P_μ becomes 0.32 (0.94) for the pion (kaon) parent if only the two-body decay is assumed. However, this is not the case for kaons. If all decay modes are taken into account, P_μ becomes 0.54 for the kaon parent [5].

If the power spectrum of the parent mesons is fixed, the polarization of the cosmic-ray muons directly reflects the K/π ratio of the secondary cosmic-ray, and vice versa. Thus, the measurement of the polarization of cosmic-ray muons provides a check on our understanding of the development of the air shower.

1.3 Muon polarization and atmospheric neutrino flux

The measurement of the spin-polarization of cosmic-ray muons can also provide a check of the atmospheric neutrino flux.

The muon polarization causes the ν_e's from the muon decay to be thrown forward compared with the ν_μ's from the muon decay, which results in the ν_e's of higher energies and ν_μ's of lower energies. Then if we observe neutrinos at a fixed energy, the flux of the ν_e's becomes larger and that of the ν_μ's smaller, since the energy spectrum of cosmic-ray muons decreases with increasing energy.

In recent years, an anomaly in the ratio of atmospheric neutrino flux defined as:

$$R_\nu \equiv \frac{\nu_\mu + \bar{\nu_\mu}}{\nu_e + \bar{\nu_e}}, \tag{1.6}$$

has been observed by some underground detectors compared with the calculated one based on the standard model of the particle physics. The ratio is taken to cancel the uncertainty of the absolute flux for each lepton neutrino. In a simple scheme R_ν is expected to be about 2 if the parent meson is pion and all pions and muons decay as:

$$\begin{aligned} \pi^\pm \rightarrow \quad & \mu^\pm \quad + \nu_\mu \; (\bar{\nu_\mu}) \\ & \mu^\pm \quad \rightarrow e^\pm + \nu_e \; (\bar{\nu_e}) + \bar{\nu_\mu} \; (\nu_\mu) \end{aligned} \tag{1.7}$$

For the ratio of the observed to the calculated R_ν, however,

$$\frac{(R_\nu)_{obs}}{(R_\nu)_{cal}} \sim 0.6 \tag{1.8}$$

was reported [6, 7, 8, 9, 10, 11]. This anomaly is one phenomenon that cannot be explained within the standard model and may be related to the neutrino oscillation. Neutrino oscillation [12, 13] may be a sign of new physics because it can take place only when neutrinos have finite mass in contradiction to the standard model.

The muon polarization effect decreases the calculated ratio $(R_\nu)_{cal}$ by about 20%, at most, compared with the unpolarized case. Thus, muon polarization is necessarily taken into account in every recent calculation of the atmospheric neutrino flux [14, 15, 16, 17, 18, 19, 20].

1.4 Status of previous experiments

The polarization of cosmic-ray muons has been measured by many experiments for energies below a few GeV in 1950's to 1970's. The aim of these experiments was to determine the K/π ratio or the energy spectrum of pions and kaons of the secondary cosmic-ray [21, 22, 23, 24, 25, 26, 27, 28, 29]. In all these experiments, the polarization was obtained by measuring the decay asymmetry of muons that came to rest in a feeble magnetic metal absorber such as copper or aluminum. Recently in the Kamiokande-II water Čerenkov detector [30], the polarization for about 1 TeV was obtained by measuring an angle between the direction of the muon and its decay electron event-by-event. For the energy range from 10 GeV to 1 TeV and above 1 TeV, no measurement has been done yet.

1.5 Motivation of this experiment

Since an anomaly of the atmospheric neutrinos has been observed at around 1 GeV (or less) and around 7 GeV, measuring the spin-polarization of cosmic-ray muons around these momentum regions is important. However, the results of the previous experiments greatly differ from each other and no recent measurement exists around 1 GeV with well-calibrated detectors with polarized muon beams. Additionally, one measurement [24] has been done around 10 GeV and the result of that was much smaller than the expectation. For these reasons, we have measured the spin-polarization of cosmic-ray muons employing a detector calibrated with the artificially produced beam muons of known polarization.

The measurements have been done at Akeno and Ohya observatories of Institute for Cosmic Ray Research, University of Tokyo, employing the same detector. The lower limits of the observable energy of cosmic-ray muons are about 1 GeV and 14 GeV for each site, respectively.

In Chapter 2, the principle of the measurement, the detector, and its data-taking system are described. The beam test for the detector was done at the BOOM facility at KEK. The results of the beam test are described in Chapter 3. A brief description of each experimental site is given in Chapter 4. In Chapter 5, a procedure for the determination of the polarization is described, and depolarization and systematic errors are quantitatively estimated. The results of the measurement are summarized with those of the previous experiments in Chapter 6. Comparison with the previous experiments, and an estimate of the muon polarization effect on the atmospheric neutrino flux is given in Chapter 7. Finally, conclusions of this experiment are given in Chapter 8.

Chapter 2

Measuring techniques

2.1 Principle of the measurement

The longitudinal polarization of cosmic-ray muons was measured by stopping the muons in an aluminum absorber plate and observing a statistical up-down asymmetry of its decay electrons detected by scintillation counters just above and below the absorber. A schematic view of the fundamental part of the detector, which we call a *detector unit* in this paper, is shown in Figure 2.1.

The muon decays via a week interaction with a 100% branching-ratio as:

$$\mu^{\pm} \rightarrow e^{\pm} + \nu_e(\bar{\nu}_e) + \bar{\nu}_\mu(\nu_\mu) \tag{2.1}$$

In this decay, the parity invariance is not hold and the angular distribution of the decay leptons depends on the direction of the muon spin. The decay matrix of the spin-polarized muon is written as [31]:

$$\mathcal{M} = \frac{G_F}{\sqrt{2}}\left[\bar{\nu}_\mu \gamma^\sigma (1-\gamma^5)\frac{1+\gamma^5 \cdot \not{s}}{2}\mu\right]\left[\bar{e}\gamma_\sigma(1-\gamma^5)\nu_e\right], \tag{2.2}$$

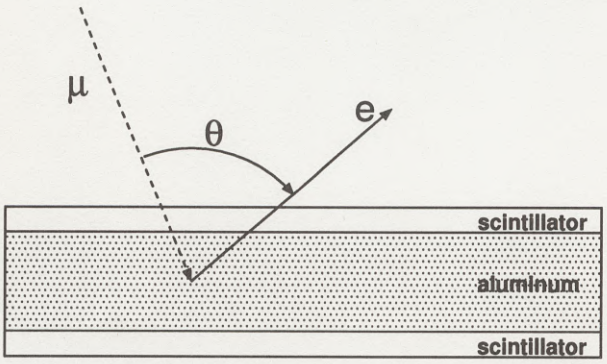

Figure 2.1: Schematic view of the *detector unit*. The definition of the decay angle θ is shown.

	$f_0(x)$	$f_1(x)$
ν_μ,e	$2x^2(3-2x)$	$2x^2(1-2x)$
ν_e	$12x^2(1-x)$	$12x^2(1-x)$

Table 2.1: Functions for the muon decay distribution. f_i are normalized so that $\int_0^1 f_0(x)dx$=1.

where G_F is the coupling constant of the weak interaction, s is the polarization four pseudovector, and each particle represents the field. The decay spectrum of a $\mu^\pm$ at rest is calculated from Eq.(2.2) as:

$$g(x,\theta,P_\mu) \equiv \frac{d^2N}{dx\,d(\cos\theta)} = f_0(x) \mp f_1(x)\cdot P_\mu \cdot \cos\theta, \tag{2.3}$$

where x $(0 \leq x \leq 1)$ is a normalized energy of the decay lepton, P_μ is the polarization of the muons, θ is the angle between the momentum direction of the decay lepton and the spin direction of the muon (See Figure 2.1), and the function $f_i(x)$ is given in Table 2.1. The normalized energy, x, is:

$$x \equiv \frac{2E_l^*}{m_\mu}, \tag{2.4}$$

where E_l^* is the energy of the decay lepton.

From Eq.(2.3), the polarized muons are expected to give an angular distribution of electrons of the form:

$$1 + a \cdot P_\mu \cdot cos\theta, \tag{2.5}$$

where a is an asymmetry coefficient depending on both the electron energy and the experimental design. Thus, the decay electrons tend to be emitted to the (opposite) direction of the polarization, if a is positive (negative).

Decay asymmetry, the quantity to be measured in this experiment, is:

$$A \equiv \frac{N_u - N_d}{N_u + N_d}, \tag{2.6}$$

where N_u (N_d) is the number of decay electrons detected in the upper (lower) counters. The decay asymmetry is quantitatively related to the polarization of the muons as follows.

If N_{stop} muons stop in the absorber and $N^\pm$ muons have the helicity ± 1 ($N_{stop} = N^+ + N^-$), the number of events detected in the upper or lower counters (N_u or N_d, respectively) can be estimated with the help of a Monte Carlo simulation for the detector as:

$$\begin{pmatrix} N_u \\ N_d \end{pmatrix} = \begin{pmatrix} n_u/n_s & n_d/n_s \\ n_d/n_s & n_u/n_s \end{pmatrix} \begin{pmatrix} N^+ \\ N^- \end{pmatrix}, \tag{2.7}$$

where n_s is the number of decay electrons generated in the Monte Carlo simulation for 100% polarized muons, n_u (n_d) is the number of decay electrons detected in the upper (lower) counter in the Monte Carlo simulation ($n_s \geq n_u + n_d$). Substituting Eq.(2.7) in Eq.(2.6), the decay asymmetry is given as:

$$A = \frac{n_u - n_d}{n_u + n_d} \cdot \frac{N^+ - N^-}{N^+ + N^-} \equiv A_1 \cdot P_\mu, \tag{2.8}$$

where A_1, which we call an effective asymmetry coefficient in this paper, is the decay asymmetry for the 100% polarized muons. Thus, the decay asymmetry is proportional to the polarization of the parent muons.

The negative muons at rest in the aluminum absorber rapidly form muonic atoms and, consequently, are rapidly depolarized [32]. The angular distribution of the μ^-'s at rest is nearly isotropic. Some captured μ^-'s are absorbed by the nuclei via the weak interaction before they decay, which makes the life time of μ^- ($\equiv \tau^-$) shorter than that of μ^+ ($\equiv \tau^+$), where [2, 33]

$$\begin{aligned} \tau^+ &= 2.19703 \pm 0.00004\ \mu s \\ \tau^- &= 0.8640 \pm 0.0010\ \mu s \end{aligned} \tag{2.9}$$

Using this difference of the life time, μ^+ and μ^- were statistically distinguished in an off-line analysis.

2.2 Detector and the data-taking system

A schematic view of the detector is shown in Figure 2.2. It contains nine *detector units*. A *detector unit* consists of a $750 \times 250 \times 40\ mm^3$ aluminum plate and two $750 \times 250 \times 10\ mm^3$ scintillators just above and below the aluminum plate. The upper two aluminum layers were used as a filter to stop low energy backgrounds such as the cosmic-ray electrons and environmental radiation. Note that some scintillators (**3-5**, **13-15**) were used as both the upper and the lower counters of the *detector unit* simultaneously. The main part of the detector was surrounded by four anticounters. All scintillation counters had the same size.

2.2.1 Detector components

Aluminum was selected as the absorber because it is a stable material, has feeble magnetism, a spin-relaxation time which is long compared with the life time of the muon, and is strong against temperature changes. In most of previous experiments copper was used as the absorber. Though copper has also these characteristics, the spin-relaxation time of aluminum is longer than that of copper and is also stronger against temperature change [34]. Additionally, the square mean of the scattering angle of the decay electrons in aluminum is smaller than that in copper because the radiation length of aluminum is longer than that of copper. Aluminum A1050 of Japanese Industrial Standard (JIS) was used in this experiment. The components of A1050 are listed in Table 2.2 [35]. The purity is more than 99.5%.

A schematic view of a scintillation counter is shown in Figure 2.3. The plastic scintillator of Bicron BC-412 [36] and Kraray SCSN81 [37] was used. For example, an attenuation time of the scintillation light of BC-412 is 3.3 ns, which is short enough compared with the life time of the muon.

The readout of the scintillator was done by a 1.5 inch diameter photomultiplier tube (PMT), Hamamatsu R580 [38], through a fish-tail shaped lightguide manufactured

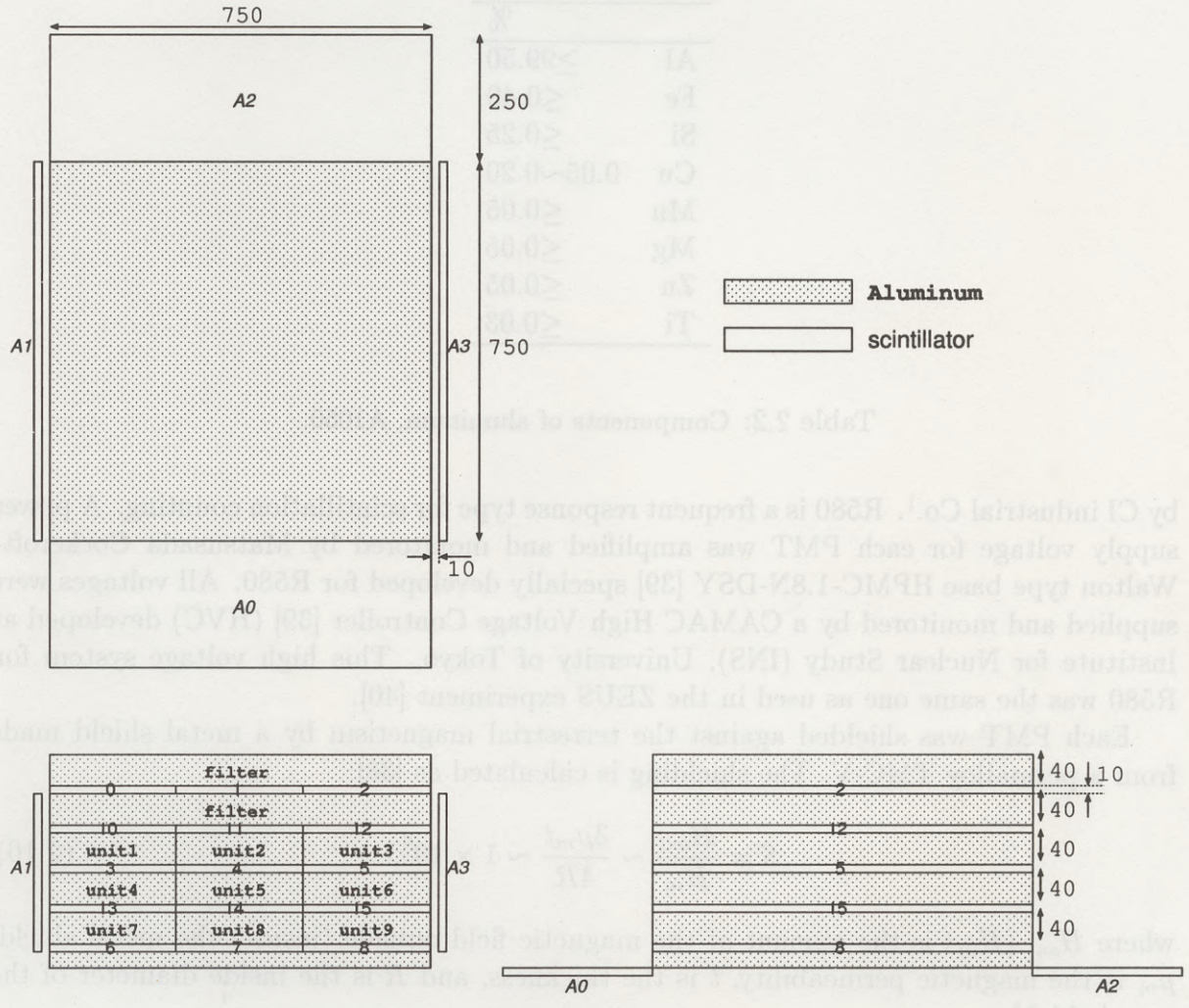

Figure 2.2: Schematic view of the detector. The lower two figures are side views and the upper one is top view. The bold number assigned for each scintillator is the counter number. **0-15** are main counters and **A0-A3** are anticounters. The unit of a scale is *mm*.

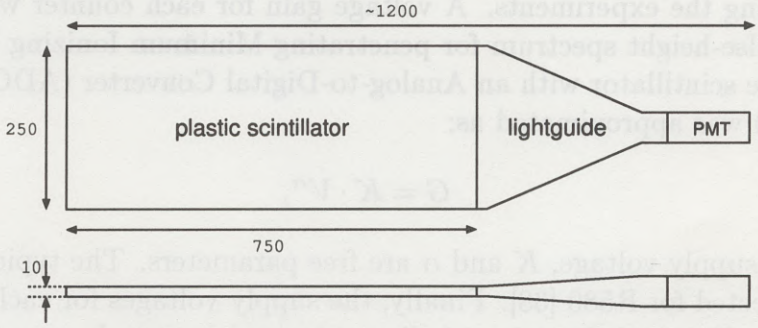

Figure 2.3: Schematic view of a scintillation counter. The unit of the scale is *mm*.

	%
Al	$\geq$99.50
Fe	$\leq$0.40
Si	$\leq$0.25
Cu	0.05$\sim$0.20
Mn	$\leq$0.05
Mg	$\leq$0.05
Zn	$\leq$0.05
Ti	$\leq$0.03

Table 2.2: Components of aluminum, A1050.

by CI industrial Co.[1]. R580 is a frequent response type for scintillation counting. A power supply voltage for each PMT was amplified and monitored by Matsusada Cockcroft-Walton type base HPMC-1.8N-DSY [39] specially developed for R580. All voltages were supplied and monitored by a CAMAC High Voltage Controller [39] (HVC) developed at Institute for Nuclear Study (INS), University of Tokyo. This high voltage system for R580 was the same one as used in the ZEUS experiment [40].

Each PMT was shielded against the terrestrial magnetism by a metal shield made from a permalloy TMC-V. The shielding is calculated as [38]:

$$S = \frac{H_{out}}{H_{in}} \sim \frac{3\mu_m t}{4R} \sim 1 \times 10^5, \tag{2.10}$$

where H_{out} (H_{in}) is the amount of the magnetic field outside (inside) the metal shield, μ_m is the magnetic permeability, t is the thickness, and R is the inside diameter of the metal shield.

2.2.2 Counter tests

The lower limits of the supply voltages ($\equiv V_{min}$), which were high enough to satisfy almost 100% detection efficiency, were measured for all counters with penetrating cosmic-rays before performing the experiments. A voltage gain for each counter was determined by measuring a pulse-height spectrum for penetrating Minimum Ionizing Particle (MIP) at the center of the scintillator with an Analog-to-Digital Converter (ADC), Hohshin C009. The gain ($\equiv G$) was approximated as:

$$G = K \cdot V^{\alpha}, \tag{2.11}$$

where V is the supply voltage, K and α are free parameters. The typical value of α was about 6 as expected for R580 [38]. Finally, the supply voltages for each counter were set to be more than V_{min} and the gains of all counters were set to be equal.

[1] 2-674-2, Mikajima, Tokorozawa-shi, Saitama 359, Japan

The position dependence of the pulse-height of the output signal of the PMT was measured for some counters using a small trigger counter with dimensions of 50×50×5 mm^3. The scintillator was equally divided into nine regions and the cosmic-rays were penetrated at the center of each region. The attenuation of the peak pulse-height of the MIP spectrum between two most separated positions was about 10%, which agrees with that the attenuation length of the scintillator is 400cm.

Some after-pulses of PMT were observed for some counters on a few μs after the first pulse when the supply voltage was more than 1500 V that was near the upper limit of the allowed voltage. These pulses become a critical background because they mimic the decay events. Thus, the supply voltage was set to be less than 1500 V for all counters, even for bad counters of smaller gain.

2.2.3 Data-taking system

A block diagram of the data-taking system is shown in Figure 2.4. The output signals of each PMT were first converted to NIM-level signals by discriminators whose thresholds were set to be about 50% of the MIP peak. Then they were finally arranged as a trigger signal and monitor signals through the logical circuit constructed with NIM modules as shown in Figure 2.5.

The cosmic-ray muons coming from above were considered to have stopped in the absorber, if a coincidence signal of the upper two counters did not have any signals from the lowest one or the anticounters. The trigger signal was generated then and was sent to both CAMAC Time-to-Digital Converter (TDC), Hohshin C006, and CAMAC coincidence register, Kaizu 3220.

For each triggered event, a time difference between the muon incoming and the next hitting in the counter of **3-8**, **10-15** was measured by the TDC whose time resolution is 5 ns. Simultaneously, the counters penetrated by the incoming muon were recorded by the register. Data were taken for the case in which at least one stop-signal was detected within a recorded time band of the TDC (20 μs). A probability of the muon decay within the recorded time band is given as:

$$1 - exp\left(-\frac{t_w}{\tau}\right) \geq 99.99\%, \tag{2.12}$$

where t_w is the recorded time band and τ is the life time of the muon.

Since the TDC used in this experiment was of a single-stop type, the start-signal was delayed by about 0.2 μs compared with the stop-signal in order not to trigger the signal of the incoming muon by itself. About 9 (20)% of the decay events of μ^+ (μ^-) were lost by this condition. To avoid a double trigger of the TDC, each trigger signal was followed by a busy signal of 100 μs width. The pulse timing in the circuit is summarized in Figure 2.6, Figure 2.7, and Figure 2.8.

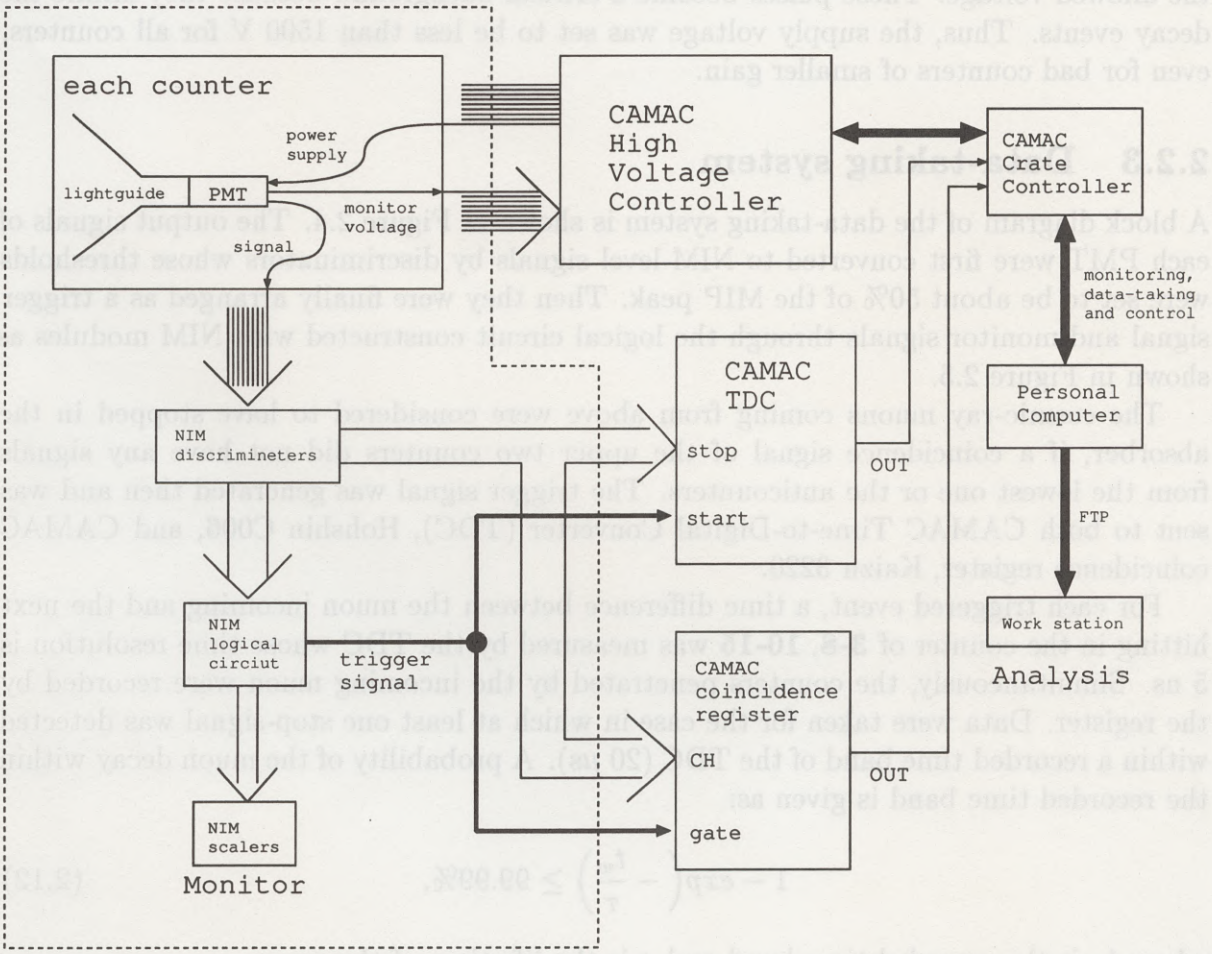

Figure 2.4: Block diagram of the data-taking system. The surrounded region by the dashed line is magnified in Figure 2.5.

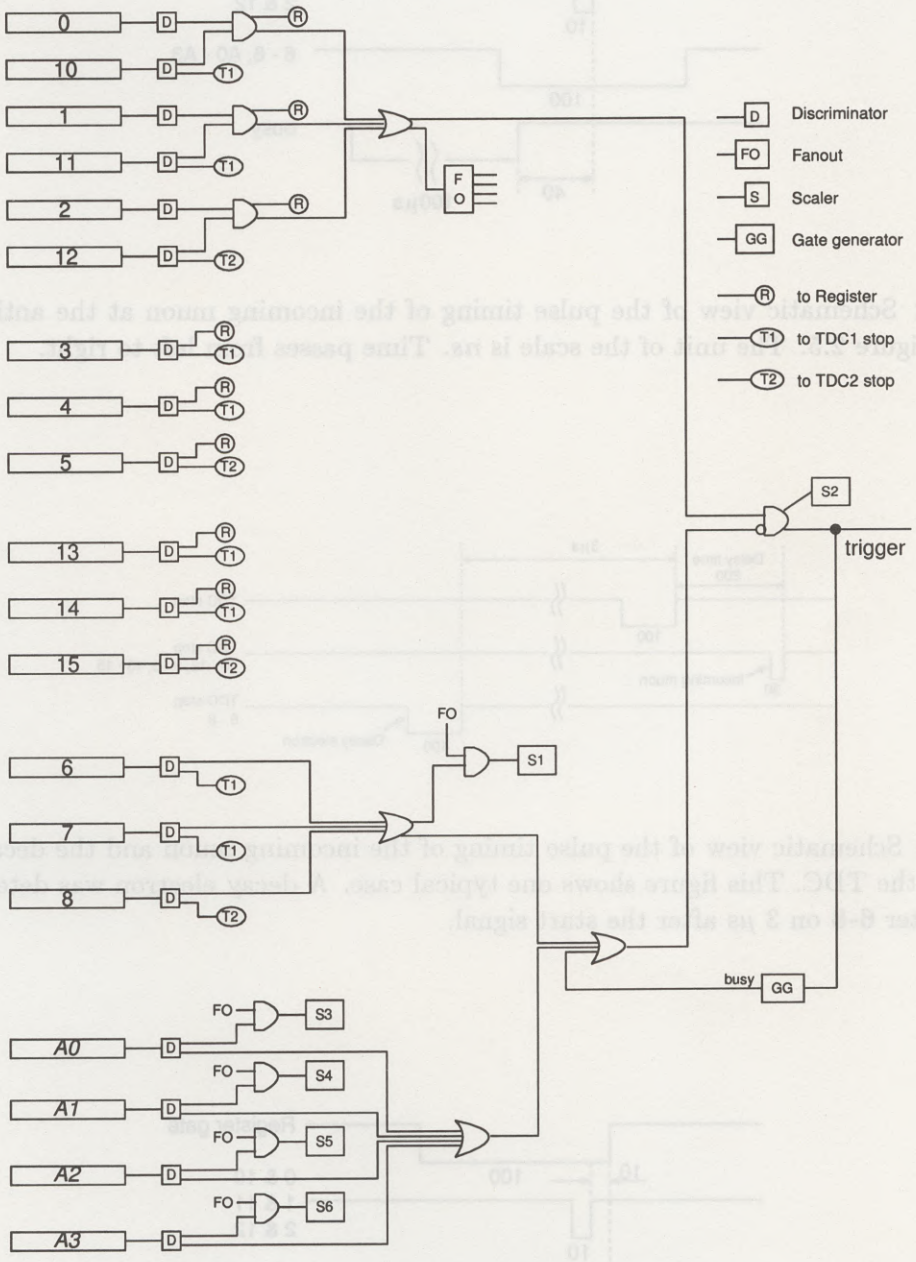

Figure 2.5: Schematic view of the trigger logic constructed with NIM modules. The bold numbers on the left side correspond to the counter number.

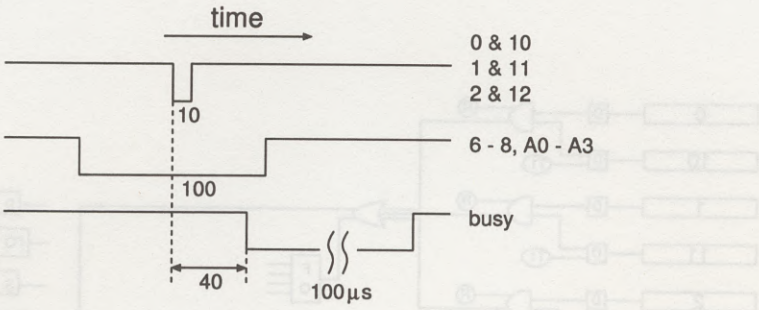

Figure 2.6: Schematic view of the pulse timing of the incoming muon at the anticoincidence circuit in Figure 2.5. The unit of the scale is *ns*. Time passes from left to right.

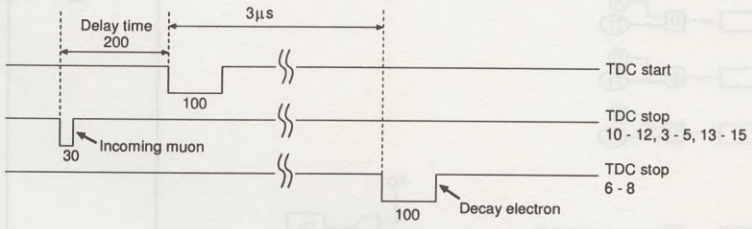

Figure 2.7: Schematic view of the pulse timing of the incoming muon and the decay electrons just before the TDC. This figure shows one typical case. A decay electron was detected in one of the counter **6-8** on 3 μs after the start signal.

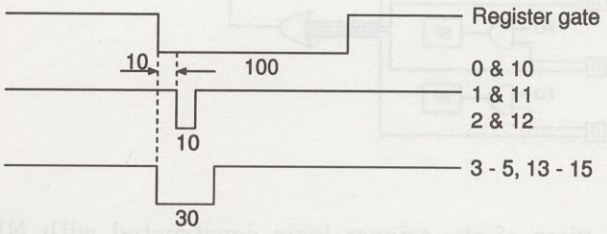

Figure 2.8: Schematic view of the pulse timing of the incoming muon just before the coincidence register.

To cancel an up-down asymmetry of the counter gains, settings of the counters were periodically changed as:

$$\begin{array}{rcl} \textit{Setting 1} & & \textit{Setting 2} \\ (\mathbf{10,11,12}) & \leftrightarrow & (\mathbf{6,7,8}), \\ (\mathbf{3,4,5}) & \leftrightarrow & (\mathbf{13,14,15}), \end{array} \tag{2.13}$$

where bold number denotes the counter number. Figure 2.2 shows the *Setting 1.*

The supply voltage for each PMT was monitored at the beginning and the end of every run by the HVC. It was very stable during the measurement. The fluctuation of the supply voltage was about ± 0.5 V for each counter at both experimental sites. The fluctuation of the PMT gain by this fluctuation of the voltage is negligible. During measurements, the output rate of each counter was also monitored by scalars as shown in Figure 2.5.

In an off-line analysis, a correlation between the outputs of the TDC and a sequence time of the measurement was checked for each counter. Any malfunction of the PMT, if any, could be found during the measurement, however which did not happen.

2.2.4 Construction of the detector

Since the detector could be disassembled and the weight of each piece was less than 15 kg, carrying and setting of the detector could be done easily. As for setting the detector, the aluminum shelf was fabricated at first, then counters except anticounters were inserted in it. Four anticounters were placed around the aluminum shelf. The aluminum shelf was geometrically well reproducible.

There was a slack to insert the counters into the shelf smoothly. The vertical slack was 4 mm and the horizontal one was about 3 mm per each counter.

The multiple layer design made us save experimental space and the number of counters while increasing the effective area.

Chapter 3

Beam tests for the detector

Before the measurement of the spin-polarization of cosmic-ray muons, the detector was tested with a polarized $\mu^{\pm}$ beam at the Booster Meson Facility [41] (BOOM) of Meson Science Laboratory, Faculty of Science, University of Tokyo in KEK. Life time and depolarization of the polarized $\mu^{\pm}$ in the aluminum absorber were measured. The position dependence of the decay asymmetry in the *detector unit* was measured and compared with a Monte Carlo simulation.

3.1 BOOM facility

A layout of the experimental hall of the BOOM is shown in Figure 3.1. The muons, the decay-products of the pions generated via the interaction of 500 MeV protons with a production target, are used as the beam. An advantage of the BOOM is that the polarized muons are used as a sharp pulse beam without a background of an accidental coincidence seen for the continuous beam muon. The frequency of the pulse beam is 20 Hz.

Two kinds of experimental ports, μ-port and π-port, are available in the BOOM. A surface muon is available at π-port, where full polarization is expected though the beam momentum is fixed. On the other hand, the beam momentum of both muon and pion can be varied at μ-port. Backward and forward muons are available as fully polarized muons by arranging a combination of the momentum of both muon and pion. The backward muon beam was used in the beam tests at μ-port, the reason of which is described later. The beam tests were done at both π1-port and μ1-port. The main beam parameters are summarized in Table 3.1 [41].

3.1.1 μ-port

The pions, which are generated in the direction of the proton beam, are sent to μ-port. The muon beam is obtained in the pion decay in about 10 m decay tunnel. Full polarization is expected by selecting the backward or forward muons defined as muons decaying in the backward or forward direction in the pion rest frame with respect to the pion momentum. For the backward (forward) muons, a momentum relationship between

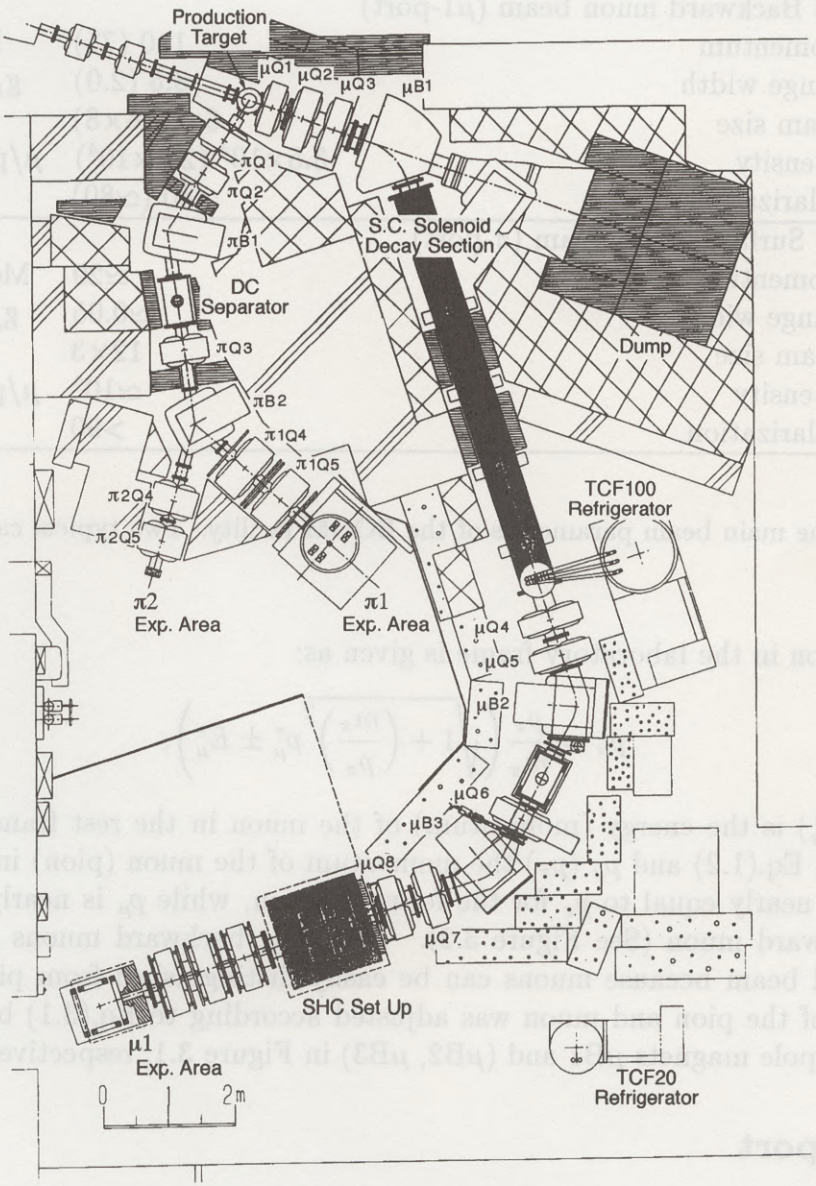

Figure 3.1: Top view of the experimental hall of the BOOM facility [42].

(a) Proton beam		
Energy	500	MeV
Pulse width	5×10^{-8}	s
Pulse frequency	20	Hz
Pulse intensity	2	μA
(b) Backward muon beam (μ1-port)		
Momentum	110 (75)	MeV
Range width	3.5 (2.0)	g/cm^2
Beam size	6×8 (6×8)	cm^2
Intensity	3.5×10^4 (2.8×10^4)	μ/pulse
Polarization	$\simeq$80 ($\simeq$80)	%
(c) Surface muon beam (π-port)		
Momentum	$\simeq$29	MeV/c
Range width	$\simeq$0.05	g/cm^2
Beam size	12×3	cm^2
Intensity	$\simeq10^4$	μ/pulse
Polarization	>90	%

Table 3.1: The main beam parameters of the BOOM facility. Two typical cases are shown at section (b).

pion and muon in the laboratory frame is given as:

$$p_\mu = \frac{p_\pi}{m_\pi}\left(\sqrt{1+\left(\frac{m_\pi}{p_\pi}\right)^2}\,p_\mu^* \pm E_\mu^*\right), \tag{3.1}$$

where E_μ^* (p_μ^*) is the energy (momentum) of the muon in the rest frame of the parent pion given in Eq.(1.2) and p_μ (p_π) the momentum of the muon (pion) in the laboratory frame. p_μ is nearly equal to p_π for the forward muon, while p_μ is nearly equal to $p_\pi/2$ for the backward muon (See Figure 3.2). Thus, the backward muons are suitable for the polarized beam because muons can be easily distinguished from pions. The beam momentum of the pion and muon was adjusted according to Eq.(3.1) by arranging the amount of dipole magnets μB1 and (μB2, μB3) in Figure 3.1, respectively.

3.1.2 π-port

The surface muons scattered at an angle of 102.5° with respect to the direction of the proton beam momentum are collected and sent to π-ports. Since the surface muon is a decay product of the pion at rest at the surface of the target, full polarization is expected. However, the spin of the beam muon tilts at a small angle with respect to the beam direction through a DC separator used for μ/e separation.

At the DC separator, a dipole electric field is applied to separate the muon and electron and a magnetic field is applied to set muon back on the right orbit. Since the spin is not affected but the orbit is bent by the electric field, the longitudinal polarization of the

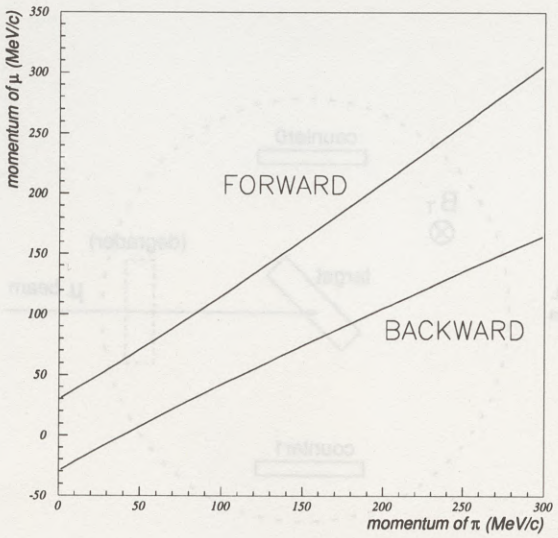

Figure 3.2: Relationship of momentum between muon and pion for the backward or forward muon.

beam muon is decreased. This reduced polarization is kept through the magnetic field because the frequency of the spin-precession and that of the cyclotron motion is almost the same for the free particle. The tilt angle ($\equiv \theta_{tilt}$) is calculated as:

$$\theta_{tilt} = \tan^{-1}\left(\frac{eVl}{m_\mu \beta^2 d}\right) \sim 9^\circ, \tag{3.2}$$

where e is the electric charge of muon, V (200 kV) is the applied voltage at DC separator, l (60 cm) is the length of the DC separator, d (10 cm) is the distance over which the voltage was applied, m_μ (106 MeV) is the mass of the muon, and β ($\sim$0.27) is the initial velocity of the muon.

3.2 Life time and depolarization of polarized muons in aluminum

As mentioned in the last chapter, the μ^- that comes to rest in the aluminum absorber is expected to be depolarized immediately. The μ^+ that comes to rest in the aluminum absorber is also expected to be depolarized due to the possibility of muonium formation and other conceivable depolarization effects [43]; however, not so much as the μ^-.

The behavior of the polarized μ^+ in the aluminum absorber was investigated under the magnetic field at π1-port, where a higher polarization is expected than at μ-port as shown in Table 3.1. The setup of the measurement is shown in Figure 3.3 and Figure 3.4. The muon beam was directly injected into a small sample ($100\times100\times20$ mm^3) of $A1050$

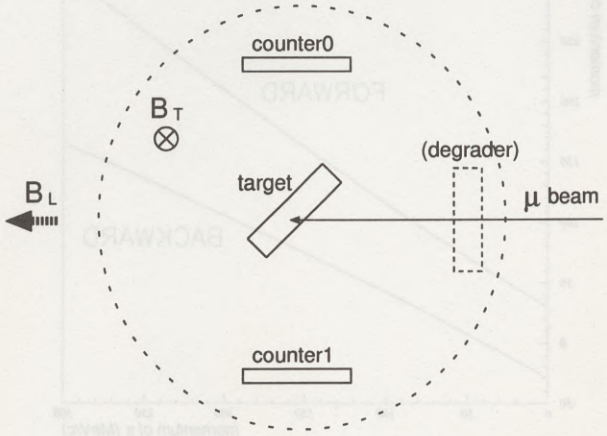

Figure 3.3: Schematic view of the setup of the measurement of the life time and depolarization of the muon at both π1- and μ1-port. The aluminum degrader in front of the aluminum target was removed (placed) at π1 (μ1)-port. The magnetic field could be applied in two directions, transverse ($\equiv B_T$) and longitudinal ($\equiv B_L$) as shown.

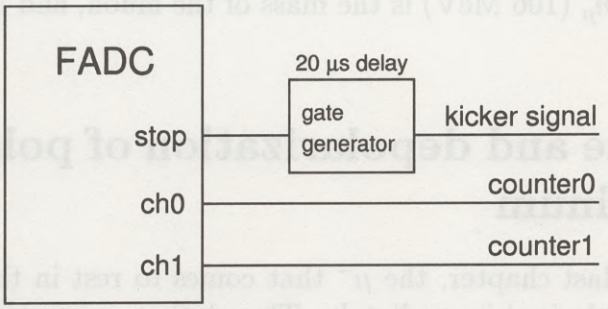

Figure 3.4: Schematic view of the data-taking system for the setup shown in Figure 3.3.

tilted at 45 ° with respect to the beam momentum. The decay electrons were detected by two scintillation counters with dimensions of 100×100×5 mm^3 at a distance of 150 mm from the sample. A transverse magnetic field of about 30 G ($\equiv B_T$) was first applied to the sample. The magnetic shield for each PMT was reinforced with a thicker metal shield when the external magnetic field was applied. Counting rates for each counter did not depend on whether the magnetic field was applied or not. Note that the *detector unit* could not be used at π-port because the surface muon comes to rest in the front scintillator and never reach into the aluminum absorber.

The time difference between the arrival time of the beam muon and its decay time was measured with a 500MHz Flash Analog-to-Digital Converter (FADC) developed at KEK [44]. The FADC was used to cope with the pulse muon beam effectively. Multiple decay events within a recorded time band of the FADC (~16 μs) could be taken together. Linearities of the FADC are shown in Figure 3.5.

Triggering was done with a kicker signal synchronized with the timing of the beam bunch. The FADC keeps sampling a pulse shape of two channels, CH0 and CH1, respectively. When a stop-signal is inserted, these data sampled within the last 16 μs are put out. A typical output of the FADC is shown in Figure 3.6. Peak searching was done as follows. A pulse was defined as a set of continuous points whose pulse-heights were larger than the threshold that was set to be about 30% of the MIP peak. The peak timing of each pulse was calculated as the mean value weighted with the pulse height.

Decay time spectra for the reconstructed pulses are shown in Figure 3.7. A spin-precession of μ^+ was observed for both counters. The phase of each precession is shifted by 180 ° each other (See A and B in the figure). A below function was fit to a sum spectrum ($C \equiv A + B$ in the figure) as:

$$\frac{dN}{dt} = N_0 \cdot exp\left(-\frac{t}{\tau}\right) + Const, \tag{3.3}$$

where N_0, $Const$, and τ are free parameters. The fitting region of the delay time was limited from 3 μs to 10 μs in the time scale of the figure. Data of early timing was not used to avoid pileup events. Data of later timing was also not used because of bad statistics. τ corresponds to the life time of the muon and was 2.23±0.01 μs, which agrees with an experimental data published in literature [2].

The subtracted time spectrum between both channels was normalized as:

$$D \equiv \frac{A - B}{A + B} \tag{3.4}$$

This corresponds to the time development of the decay asymmetry between two counters. The spin-relaxation time of μ^+ in the aluminum absorber was obtained by fitting the spectrum D with:

$$A(t) = A^T_{\pi 1} \cdot exp\left(-\frac{t}{T}\right) \cdot cos2\pi(\omega \cdot t + \zeta) + Const, \tag{3.5}$$

where $A^T_{\pi 1}$, T, ω, ζ, and $Const$ are free parameters. The spin-relaxation time was T=53^{+84}_{-19} μs, which was long enough compared with the life time of the muon. The amplitude and the frequency of the precession were $A^T_{\pi 1}$=0.258±0.015 and ω=0.42±0.06 μs^{-1}, respectively.

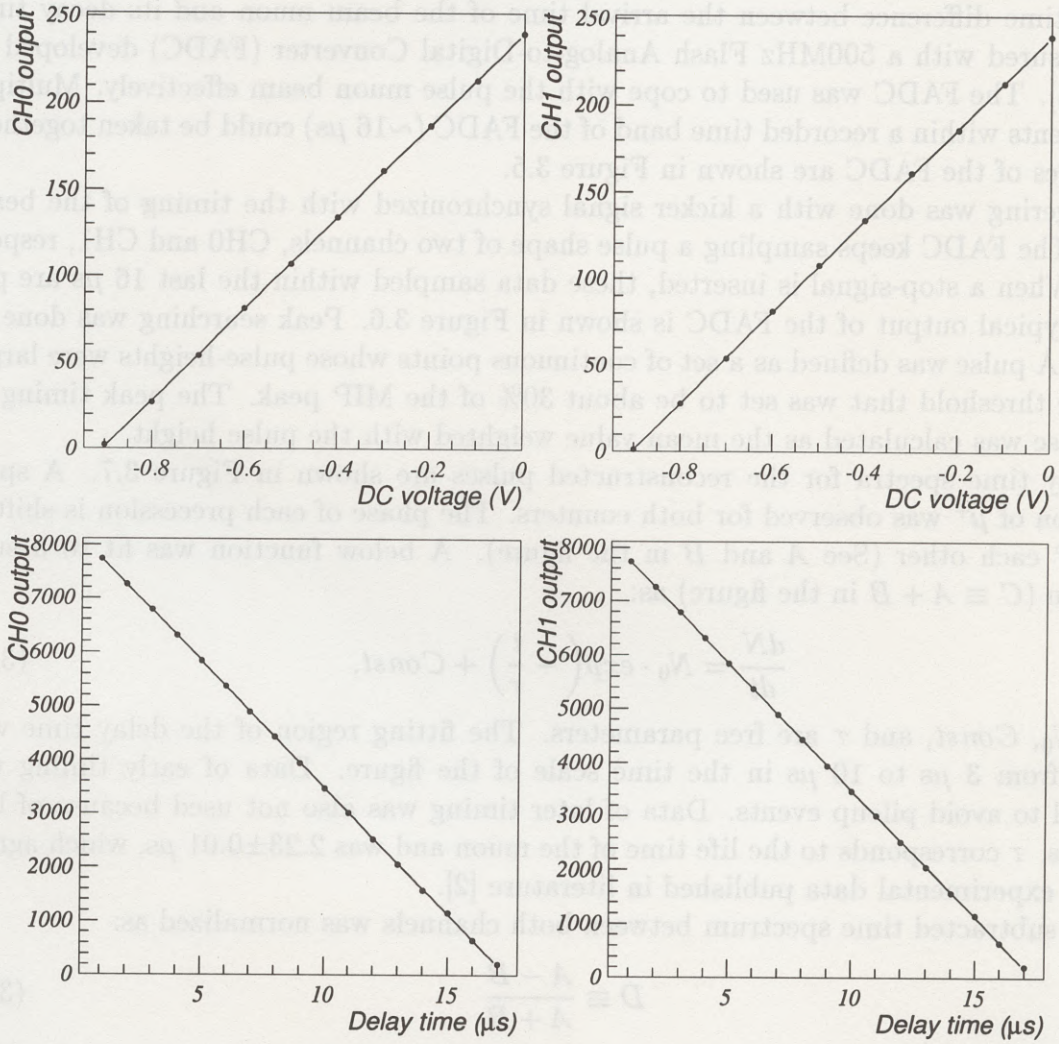

Figure 3.5: Linearities of the FADC. The upper (lower) figures show the pulse height (timing) linearity for each channel. A straight line was fit to the data.

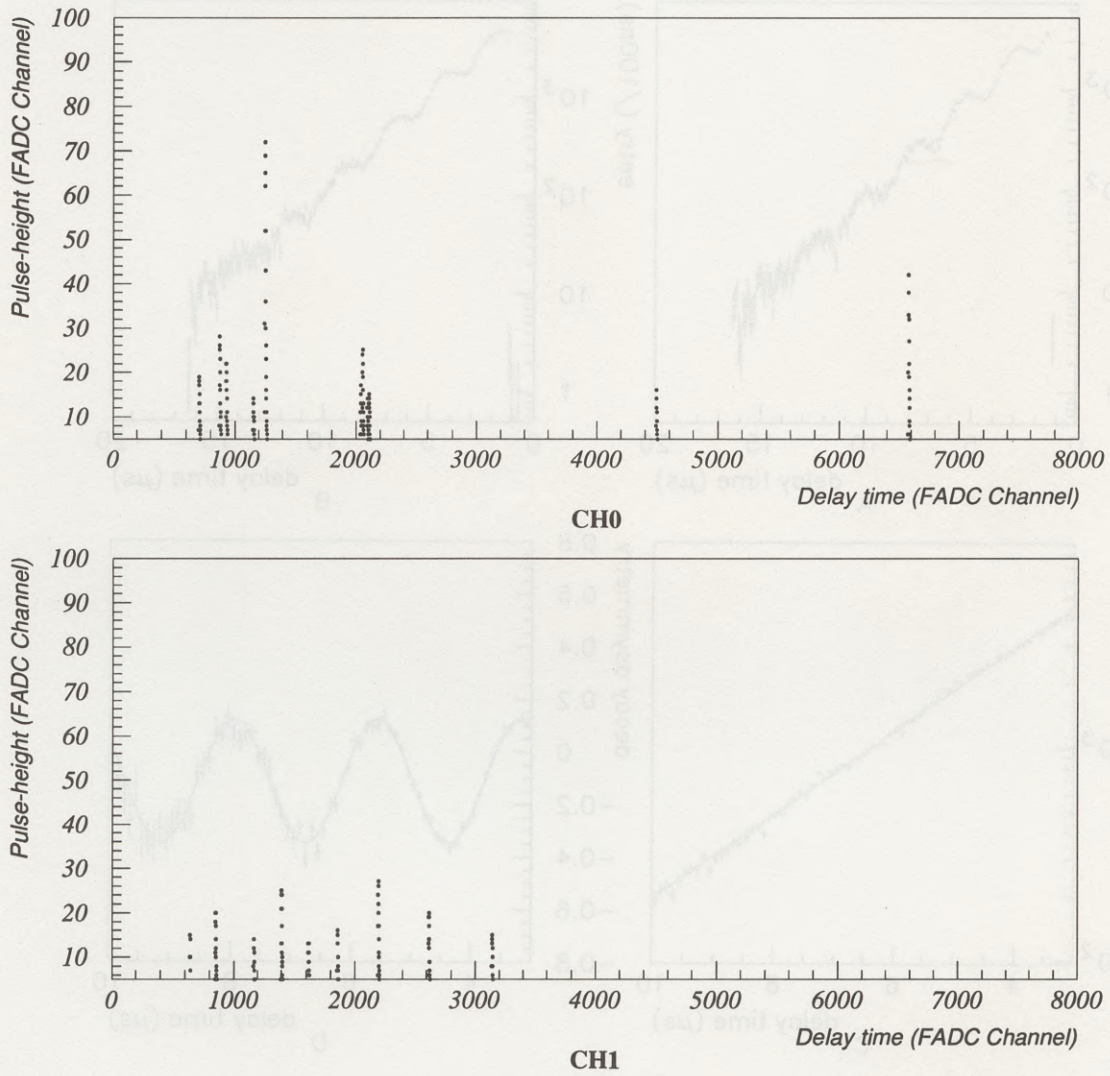

Figure 3.6: A typical output of the FADC for both channels. Multiple decay events per one trigger are shown. The units of the scale are 2 ns/CH for the horizontal axis and ~3.77 mV/CH for the vertical axis.

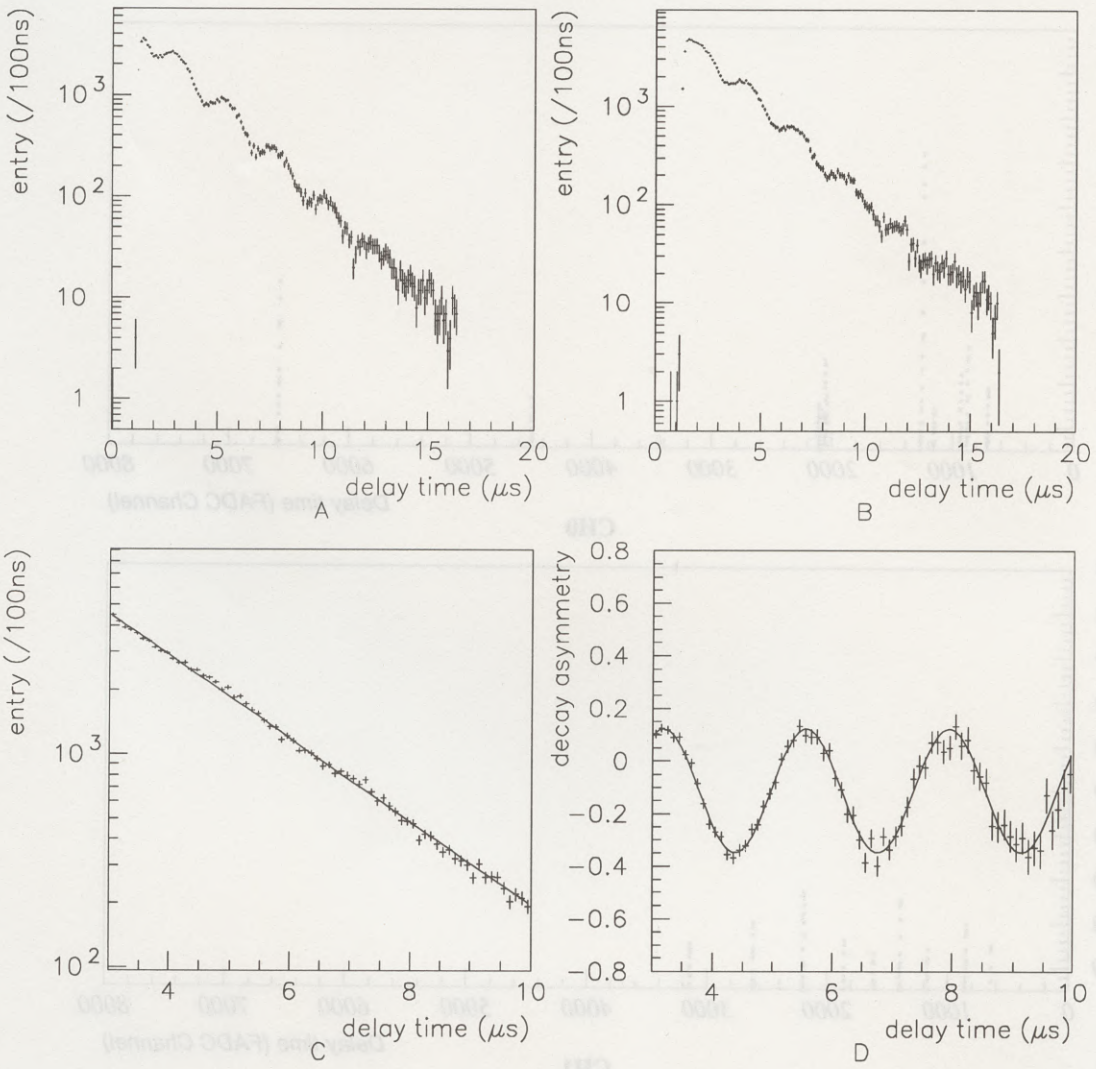

Figure 3.7: The decay time spectra of the surface μ^+'s at π1-port under transverse magnetic field. A : The decay time spectrum of counter 0, B : The decay time spectrum of counter 1, C : A+B, and D : (A−B)/(A+B). The cross bars are the entries and the solid lines are the fitting results.

The frequency of the precession is proportional to the amount of magnetic field as:

$$B = \frac{\omega}{g \cdot \mu'_B}, \tag{3.6}$$

where g ($\simeq$2) is Lande g-factor, $\mu'_B \equiv \frac{m_e}{m_\mu}\,\mu_B$, m_e (m_μ) is the mass of the electron (muon) and μ_B (=9.274$\times$10^{-24} J$\cdot$T^{-1}) the Bohr magneton. Substituting the value of ω in Eq.(3.6), B becomes 31$\pm$4 G, which was consistent with a coarse setting of the field.

The behavior of the μ^- in the aluminum absorber was investigated at μ1-port, since the μ^- beam was not available at π1-port. The same setup was used at μ1-port as shown in Figure 3.3 and Figure 3.4. The decay time spectra of the μ^- are shown in Figure 3.8. The precession was scarcely observed for the μ^-; in other words, the stopping μ^- in the aluminum absorber was almost depolarized. The life time of μ^- in the aluminum absorber was 0.82$\pm$0.07 μs, which agrees with the published data.

To measure the tilt angle of the spin of the beam muon, a longitudinal magnetic field of about 30 G ($\equiv B_L$) was applied at π1-port. The time spectra of the μ^+ under the longitudinal magnetic field are shown in Figure 3.9. A slight precession was observed. The life time of μ^+ in the absorber was 2.22$\pm$0.03 μs, which agrees with the published data. The precession amplitude was $A^L_{\pi 1}$=0.065$\pm$0.022. Taking the ratio of the amplitude obtained under longitudinal to transverse magnetic field, the tilt angle at π1-port was calculated as:

$$\theta_{tilt} = sin^{-1}\left(\frac{A^L_{\pi 1}}{A^T_{\pi 1}}\right) = 15 \pm 6^\circ, \tag{3.7}$$

which agrees with the expected value as shown in Eq.(3.2). Consequently, the beam polarization at π1-port was:

$$P_{\pi 1} = cos(\delta_{tilt}) = 97 \pm 3\% \tag{3.8}$$

The beam polarization at μ1-port was calibrated by measuring the precession amplitude under transverse magnetic field with the same setup of the measurement. The decay time spectra of the μ^+ at μ1-port under transverse magnetic field are shown in Figure 3.10. The life time and the precession amplitude were 2.15$\pm$0.01 μs and $A^T_{\mu 1}$=0.194$\pm$0.023, respectively. The beam polarization of μ1-port was:

$$P_{\mu 1} = \frac{A^T_\mu}{A^T_\pi} \cdot P_{\pi 1} = 73 \pm 10\%, \tag{3.9}$$

which agrees with the expected value as shown in Table 3.1.

3.3 Position dependence of the decay asymmetry

The detector response for the polarized muons was investigated at μ1-port with a *detector unit*. The setup of the measurement is shown in Figure 3.11. The beam muon was perpendicularly inserted into the *detector unit* and was stopped in the aluminum absorber. The decay electron was detected by the counters, b and c. Triggering was done with a

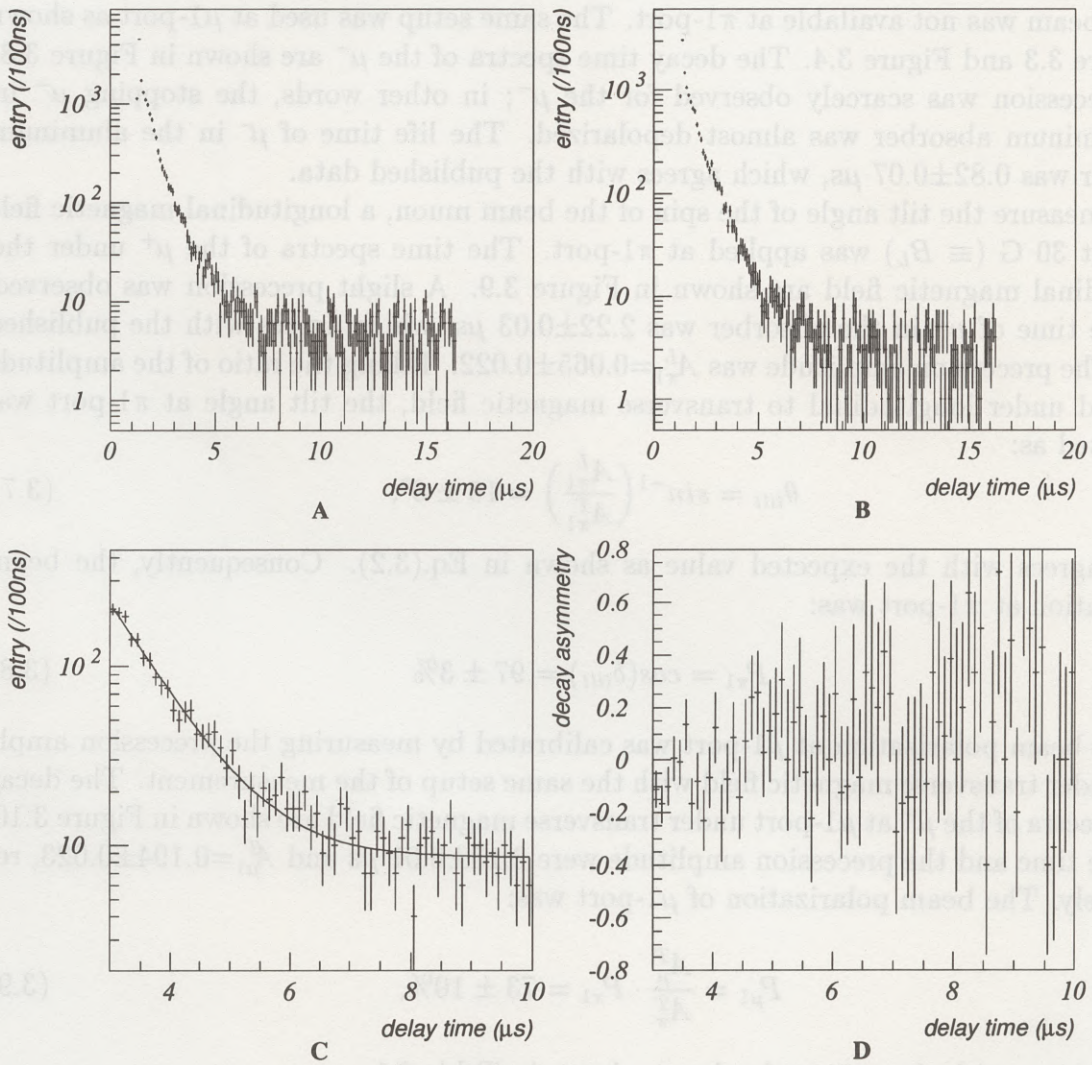

Figure 3.8: The decay time spectra of the backward μ^-'s at μ1-port under transverse magnetic field.

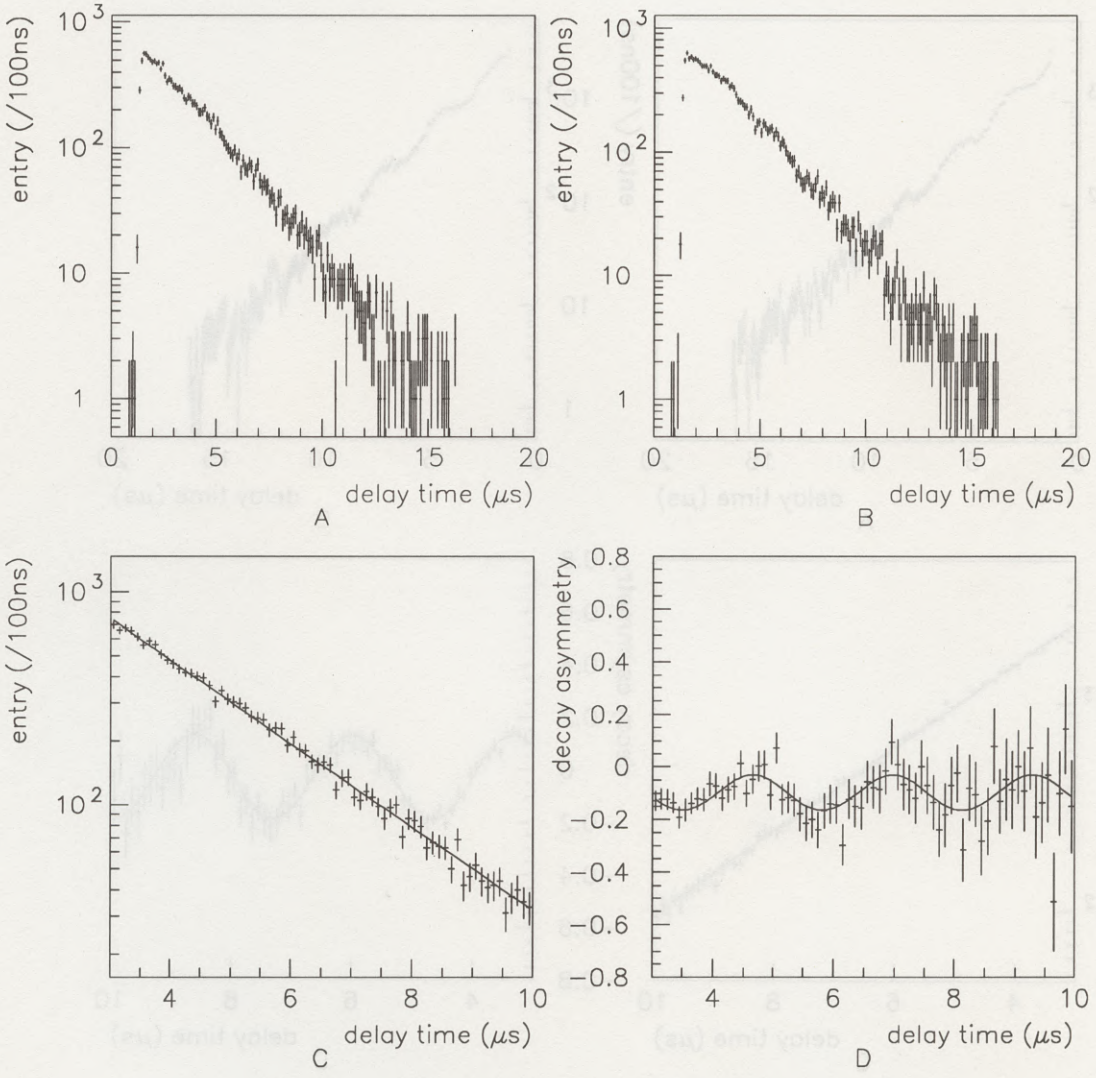

Figure 3.9: The decay time spectra of the surface μ^+'s at π1-port under longitudinal magnetic field.

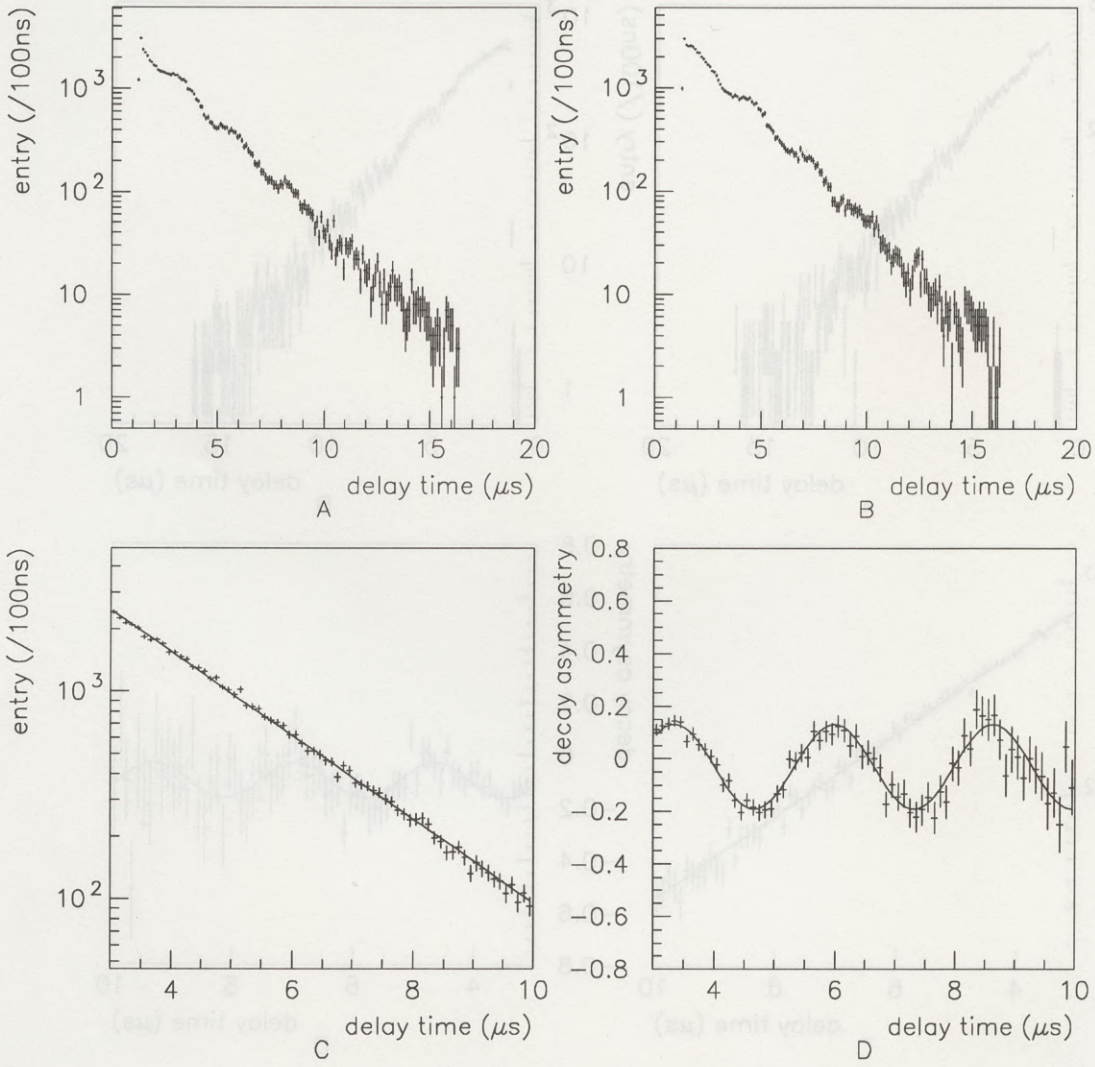

Figure 3.10: The decay time spectra of the backward μ^+'s at μ1-port under transverse magnetic field.

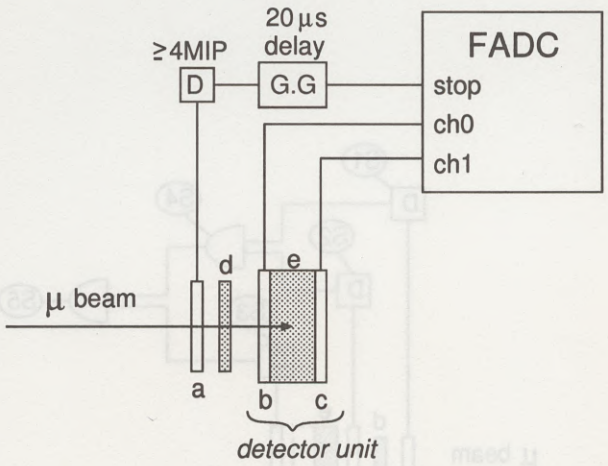

Figure 3.11: Schematic view of the setup for the measurement of the decay asymmetry for the *detector unit* at μ1-port. a is a trigger counter, b (c) is a front (rear) counter of the *detector unit*, d is an aluminum degrader, and e is an aluminum target absorber. D represents a discriminator and $G \cdot G$ represents a gate generator used as a delay module.

scintillation counter, a, with dimensions of $200\times200\times10$ mm^3 in front of the *detector unit*. The trigger threshold was set to be $4\times$(MIP peak).

The momentum of the beam muon was determined for those muons that come to rest in the middle of the 4 cm thick absorber. For this purpose, a counting rate for each counter was measured with scalers, reducing the absorber thickness to 2 cm as shown in Figure 3.12. The momentum of the muon, p_μ, was determined at the rising edge of the ratio of the scaler counting, $S5/S4$, and was set to be 91 MeV. The momentum of the pion, p_π, was set to be 177 MeV according to Eq.(3.1). This combination of momenta was fixed during whole measurements at μ1-port.

Adjusting the thickness of the aluminum degrader ($A1050$) in front of the *detector unit*, the beam muon was stopped at five different depths of the absorber as shown in Figure 3.13 (z-direction). The decay asymmetry between counter b and c was measured for each depth. The result is shown in Figure 3.14 together with that of a Monte Carlo simulation.

Both the measured and simulated decay asymmetries linearly increased with the depth. The depth dependence of the observed decay asymmetry agrees with that of the simulation except for one μ^- point (z=$-$10 mm). The difference of the decay asymmetry between the polarized and unpolarized one did not depend on the depth as expected because the decay asymmetry is proportional to the polarization that should not depend on the depth.

As observed in the beam tests, the μ^- that captured in the absorber was immediately depolarized. Comparing the decay asymmetry for 0% polarization muons (the shaded triangle) with that for the μ^- (the open triangle), the beam muons have stopped about 10 mm in front of the expected depth ($-$z direction). That might be the reason that

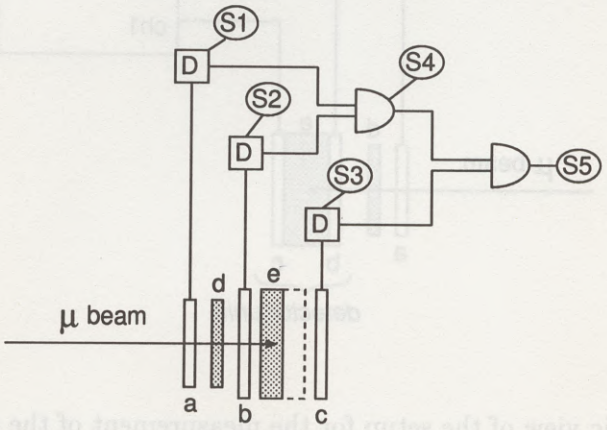

Figure 3.12: Schematic view of the setup for the rate counting. The thickness of the aluminum absorber was half of that in Figure 3.11. $S1$-$S5$ are scalers.

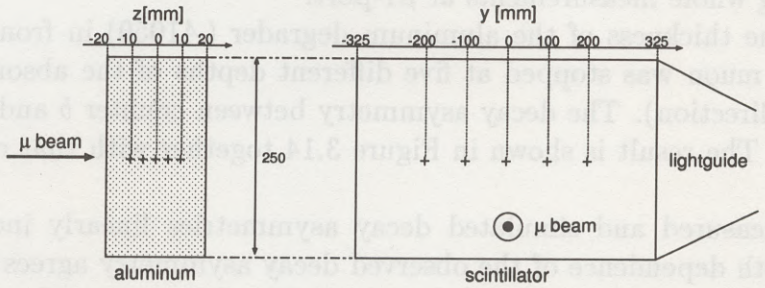

Figure 3.13: Schematic view of the stopping position of the beam muon in the aluminum absorber. Z-axis is defined toward the beam direction. Y-axis is defined along the counter length. The beam muon was stopped at around +.

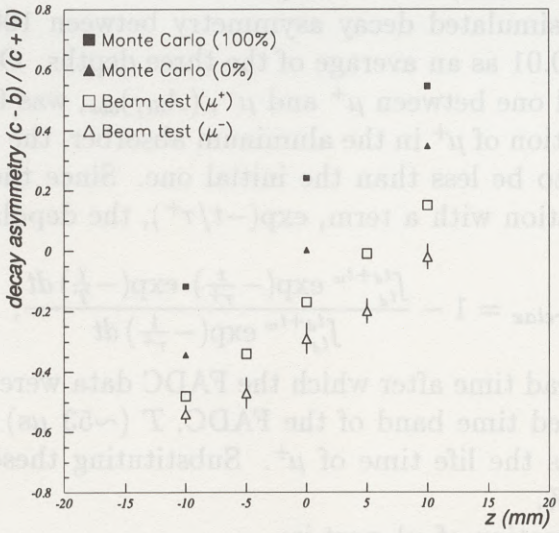

Figure 3.14: The measured and simulated decay asymmetries for each depth. The shaded rectangle shows the simulated one for 100% polarized muons, the shaded triangle shows the simulated one for 0% polarized muons, the open rectangle shows the observed one for μ^+'s, and the open triangle shows the observed one for μ^-'s.

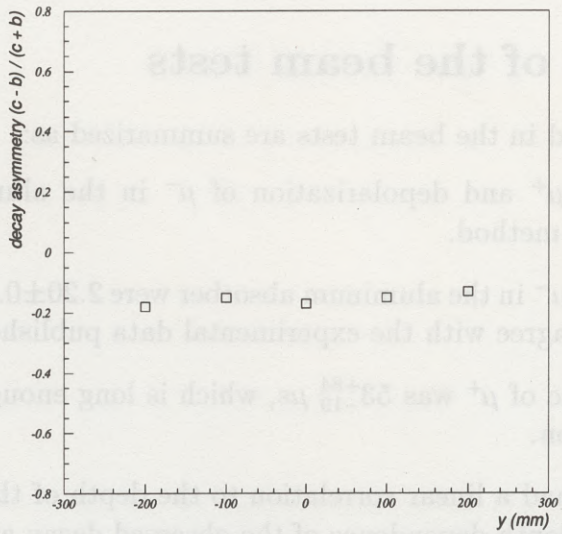

Figure 3.15: Position dependence of the decay asymmetry along the counter length.

the one point in Figure 3.14 (μ^-, z=−10 mm) deviates from the other points beyond the statistical error. These μ^-'s might leak into the front counter, *b*. Thus, we did not use these points (z=−10 mm of data) in the analysis below.

The difference of the simulated decay asymmetry between 100% and 0% polarized case, $(A_{dif})_{cal}$, was 0.22±0.01 as an average of the three depths. On the other hand, the difference of the measured one between μ^+ and μ^-, $(A_{dif})_{obs}$, was 0.15 ± 0.02.

Due to the spin-relaxation of μ^+ in the aluminum absorber, the observed decay asymmetry of μ^+ is expected to be less than the initial one. Since the observed number of decay events is an integration with a term, $\exp(-t/\tau^+)$, the depolarization is estimated as:

$$\Delta P_{relax} = 1 - \frac{\int_{t_d}^{t_d+t_w} \exp(-\frac{t}{\tau^+}) \cdot \exp(-\frac{t}{T})\, dt}{\int_{t_d}^{t_d+t_w} \exp(-\frac{t}{\tau^+})\, dt}, \tag{3.10}$$

where t_d (∼2 μs) is the dead time after which the FADC data were used for the analysis, t_w (∼16 μs) is the recorded time band of the FADC, T (∼53 μs) is the spin-relaxation time, and τ^+ (∼2.2 μs) is the life time of μ^+. Substituting these values in Eq.(3.10), ΔP_{relax} becomes about 8%.

Thus, the beam polarization of μ1-port is:

$$P_{\mu 1} = \frac{(A_{dif})_{obs}}{(A_{dif})_{cal}} \cdot \frac{1}{1 - \Delta P_{relax}} = 74 \pm 10\%, \tag{3.11}$$

which agrees with the measured one with the μSR method (See Eq.(3.9).).

A position dependence of decay asymmetry along the counter length was investigated. The beam muons were stopped at five y-positions as shown in Figure 3.13. The result is shown in Figure 3.15. The decay asymmetry did not depend on the *y*-direction.

The decay asymmetry was measured before and after changing the counter *b* and *c*. It was confirmed that the decay asymmetry did not depend on the counter exchange.

3.4 Summary of the beam tests

The main results obtained in the beam tests are summarized as:

- Spin-precession of μ^+ and depolarization of μ^- in the aluminum absorber were observed with μSR method.
- Life time of μ^+ and μ^- in the aluminum absorber were 2.20±0.02 μs and 0.82±0.07 μs, respectively. They agree with the experimental data published in literature.
- Spin-relaxation time of μ^+ was 53^{+84}_{-19} μs, which is long enough compared with the life time of the muon.
- Decay asymmetry had a linear correlation to the depth of the stopping position of the muon and the depth dependence of the observed decay asymmetry agrees with that of the Monte Carlo simulation.
- Decay asymmetry did not depend on the muon stopping position with respect to the distance from the PMT if the depth of the stopping position is fixed.

– Decay asymmetry did not depend on the counter exchange.

Chapter 4

Experimental sites

The sea-level momentum of the cosmic-ray muon was estimated as the amount of the degrader through which the muon comes to rest in the detector. The total energy loss for muons traversing matter is described by a sum of some single contributions as [45]:

$$\frac{dE}{dx} = \left(\frac{dE}{dx}\right)_i + \left(\frac{dE}{dx}\right)_b + \left(\frac{dE}{dx}\right)_p + \left(\frac{dE}{dx}\right)_n, \tag{4.1}$$

where i, b, p, and n stand for ionization, bremsstrahlung, pair production, and nuclear interaction, respectively. For energies less than 10 GeV, the dominant loss mechanism is ionization, with the other mechanism contributing only a few percent [45].

The polarization of cosmic-ray muons was measured at Akeno and Ohya observatories of Institute for Cosmic Ray Research (ICRR), University of Tokyo. The measurement was done with one same detector for both experimental sites.

Akeno Observatory [46] is at a gentle slope of Kayagatake mountains, Yamanashi Prefecture, about 900 m above sea level. Our detector was set up in one muon-station (M1) studded in the site. Since the ceiling of the muon-station is flat 2 m thick concrete (478 g·cm^2), the detector is shielded against cosmic-ray electrons. The observable lower limit of the muon energy is about 1 GeV on average. The room temperature in the muon-station is almost constant because of the thick concrete surrounding the room [47].

Ohya Observatory [48] is in the northern part of the Kanto Plain at Utsunomiya City, Tochigi Prefecture, about 149 m above sea level. A huge underground space exists at a depth of about 33 m, which was produced during the quarrying of Ohya stone. The density of Ohya stone is 1.8 $g \cdot cm^{-3}$. Our detector was set up in an experimental room in this underground space. The observable lower limit of the muon energy is about 14 GeV. Since the experimental room is in the underground and the dehumidifier system was set, the temperature in the experimental room is kept constant at all season [49].

Chapter 5

Data analysis

The polarization of cosmic-ray muons was calculated based on the data taken from May to June at Akeno and from July to November at Ohya in 1995. The number of events taken were about 10^6 and 10^5 at Akeno and Ohya, respectively.

In this section, a procedure of an extraction of the number of decay events from the raw data is described. To reduce the polarization from the observed up/down decay asymmetry, the effective asymmetry coefficient, which is the decay asymmetry for 100% polarized muons, was calculated by a Monte Carlo simulation. The depolarization of μ^+ above and in the detector and systematic errors on the polarization are estimated.

5.1 Check on the monitor rate

To check the measuring system, the counting rate monitored by the scaler was compared with theoretical expectation and the Monte Carlo simulation. The run summaries and typical counting rates are shown in Table 5.1 and Table 5.2, respectively.

The vertical intensity of cosmic-ray muons at the sea level is approximated as [50]:

$$\frac{dN}{dp} = 4.02 \times 10^{-3}\, p^{-1-0.24\ ln(p)}, \tag{5.1}$$

where p (GeV) is the momentum of the muon. The rate of the muons passing through the detector is estimated as:

$$S1 \sim \int_{E_0}^{\infty} \frac{dN}{dp}\, dp, \tag{5.2}$$

where E_0 is the lower limit of the observable energy of the muon as described in the last chapter. $S1$ was calculated as ~41 (~2.4) Hz for Akeno (Ohya) site, which was consistent with the measured one.

The trigger rate is roughly estimated as:

$$S2 \sim \frac{dN}{dp} \cdot \Delta p \cdot S, \tag{5.3}$$

where Δp (~0.15 GeV) is the momentum range for the stopping muons in the detector and S (75×75 cm^2) is the cross section of the detector. $S2$ was calculated as ~3.4 (~0.46) Hz for Akeno (Ohya) site, which was also consistent with the measured one.

RUN	*Setting*	Date	Measuring time (sec)	# of taken events
A5	1	5/14 - 5/24	875918	4×10^5
A7	2	5/25 - 6/4	861794	4×10^5
A10	1	6/5 - 6/17	1099532	5×10^5
A13	2	6/19 - 7/1	1075477	5×10^5
O3	1	7/9 - 7/18	777733	1×10^4
O4	1	7/30 - 9/3	3051475	4×10^4
O5	2	9/6 - 10/19	3717973	5×10^4
O6	2	10/22 - 11/8	1454676	2×10^4
O7	1	11/12 - 11/30	1516632	2×10^4

Table 5.1: Run summary of the measurements of the polarization of cosmic-ray muons. The upper part (A$\sim$) is for Akeno site and the lower part (O$\sim$) is for Ohya site. *Setting* means the counter setting defined in Eq.(2.13).

RUN	S1 [Hz]	S2 [Hz]	S3 [Hz]	S4 [Hz]	S5 [Hz]	S6 [Hz]
A5	36.64±0.04	3.54±0.01	3.15±0.01	–	2.14±0.01	2.47±0.01
A7	35.97±0.04	5.83±0.02	3.18±0.01	2.75±0.01	2.20±0.01	2.53±0.01
A10	36.42±0.19	3.55±0.06	3.16±0.06	2.77±0.06	2.06±0.06	2.41±0.06
A13	35.98±0.06	6.00±0.02	3.22±0.02	2.83±0.02	2.17±0.02	2.53±0.02
O3	2.78±0.01	0.25±0.01	0.22±0.01	0.24±0.01	0.19±0.01	0.20±0.01
O4	2.77±0.05	0.24±0.02	0.23±0.02	0.23±0.02	0.19±0.01	0.19±0.01
O5	2.74±0.01	0.46±0.01	0.21±0.01	0.24±0.01	0.20±0.01	0.22±0.01
O6	2.75±0.01	0.46±0.01	0.20±0.01	0.24±0.01	0.20±0.01	0.22±0.01
O7	2.80±0.01	0.25±0.01	0.20±0.01	0.24±0.01	0.19±0.01	0.20±0.01

Table 5.2: Counting rates of the scalers. Only the statistical error is quoted. The description of S1-S6 is shown in Figure 2.5. For Run A5 the scaler S4 was broken.

detector unit	A5	A7	A10	A13
1	39785	40140	49904	50460
2	40210	41105	50379	51426
3	40191	41337	50409	51357
4	32848	32190	41415	40351
5	34252	34302	43150	42278
6	35095	34344	42686	42619
7	29229	27370	36057	34586
8	29618	27957	36678	34728
9	29656	28126	36967	35057

Table 5.3: Summary of the number of events taken in each *detector unit* for each run at the Akeno site. The assign of the *detector unit* is shown in Figure 2.2.

A systematic dependence of the counting rate on the counter setting was observed for the trigger rate, S2, for both sites, which might be due to the difference of the counter gain. The rates of the anticounters, S3∼S6, did not depend on the setting, but systematically differ from scaler to scaler especially for Akeno site. The reason is discussed later. However, the data-taking rate:

$$\frac{\#\text{ of taken events}}{\text{Measuring time}} \tag{5.4}$$

did not depend on the counter setting (See Table 5.1.). Thus, it does not matter because only those events, in which the muons come to rest in the detector, were used in the analysis.

Ratios of the rate S1 to (S3∼S6) were roughly calculated by a Monte Carlo simulation, which agreed with the measured one.

5.2 Depth and lateral distributions of stopping muons

The detector was regarded as consisting of nine *detector unit*s as described in the detector section. The event, in which muon came to rest through the vertical column of the counters, was assigned to each *detector unit* using the register information.

The momentum and zenith angle distribution of the muon flux were measured using the depth and lateral distribution of the stopping muons, respectively. The number of events taken in each *detector unit* is summarized in Table 5.3 (Table 5.4) for Akeno (Ohya) sites. In both tables, the both-hit events in which the signals were detected in both the upper and lower counters simultaneously after the trigger signal were removed as background events such as the accidental coincidence of the cosmic-ray muons. In the upper *detector unit*, a larger number of entries was observed, which reflects the detector acceptance's dependence on the solid angle. Additionally, the depth dependence of the register distribution was almost the same for both sites. For example, the ratio of the

detector unit	O3	O4	O5	O6	O7
1	936	4048	4797	1911	1925
2	981	3989	5133	1973	2035
3	1008	3928	5082	2036	2024
4	809	3177	3786	1486	1630
5	944	3197	4177	1680	1601
6	907	3453	4248	1679	1693
7	666	2676	3221	1308	1447
8	676	2923	3419	1366	1436
9	752	3013	3478	1386	1497

Table 5.4: Summary of the number of events taken at the Ohya site.

Ratio of entries	Akeno	Ohya
unit5/unit2	0.841±0.003	0.822±0.010
unit8/unit2	0.704±0.003	0.696±0.009
⟨ *unit(7',9')/unit8* ⟩	0.0709±0.0003	0.073±0.009

Table 5.5: Depth and lateral distributions of the stopping muons for both experimental sites. ⟨ *unit(7',9')/unit8* ⟩ denotes an average of (*unit7'/unit8*) and (*unit9'/unit8*).

entries, (*unit5/unit2*) and (*unit8/unit2*), were about 0.84 and 0.70 for both sites as shown in Table 5.5, respectively. It might reflect the same distribution of the vertical momentum of the stopping cosmic-ray muons with the momentum from zero to a few hundred MeV/c just above the detector.

To measure the zenith angle distribution of cosmic-ray muons, some non vertical distributions as shown in Figure 5.1 were investigated. The event cluster *unit8* was defined in which the muons come to rest in *detector unit8* through the counter **1**, **11**, **4**, and **14**. The event cluster *unit7' (9')* was defined in which the muons come to rest in *detector unit7 (9)* through the counter **1**, **11**, **3** (**5**), and **13** (**15**). Both (*unit7'/unit8)* and (*unit9'/unit8)* was about 0.07 for both sites as shown in Table 5.5.

5.3 Monte Carlo simulation of the effective asymmetry coefficient

The effective asymmetry coefficient was calculated in two steps with a help of the GEANT (version 3.15) Monte Carlo package [51]. First, the distribution of the zenith angle and of the stopping positions of cosmic-ray muons was determined by comparing with the observed depth and lateral distribution. Second, the decay asymmetry was calculated by generating electrons according to Eq.(2.3).

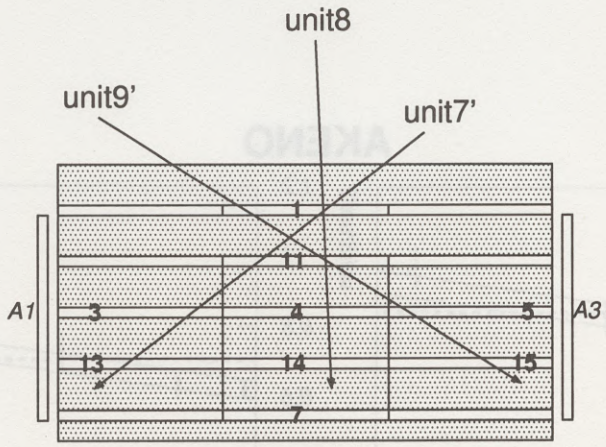

Figure 5.1: Schematic view of the non vertical flux recorded by the register. Incoming muons are demonstrated by solid arrows.

5.3.1 First step

After defining the exact geometry of the detector, muons were injected into the detector from above and the energy loss in the scintillator was calculated for each counter. The zenith angle distribution just above the detector was assumed to have a form of $cos^n\alpha$, where α is the zenith angle and n is a free parameter. Since the horizontal flux is reduced compared with the vertical flux through the degrader, the n is expected to be more than 2. The flux of the stopping muons was assumed to increase with the momentum linearly.

Passing through the same reconstruction logic of the measurement, the register distribution was obtained for the Monte Carlo events. The result is shown in Figure 5.2 and Figure 5.3. The *momentum slope* is defined as a multiplying factor of the muon flux at 500 MeV compared with that at 0 MeV. A straight line was fit to the simulated register distribution as a function of the *momentum slope* in Figure 5.2 and Figure 5.3. Taking the farthest two crossing points of the fitting curve (solid line) and the data (dashed line), the *momentum slope* was determined to be 5±2 (4±3) for Akeno (Ohya) site.

The power of the cosine of the zenith angle distribution, n, was estimated in the same way. A general exponential function;

$$P1 \cdot \exp(P2 \cdot n) + P3 \tag{5.5}$$

was fit to the simulated register distribution, where $P1$, $P2$, and $P3$ are free parameters. The n was determined to be 5.0±0.5 (5±1) for Akeno (Ohya) site.

The uncertainty of the *momentum slope* and zenith angle distribution of the muon flux will be treated as the systematic error on the polarization as discussed later.

5.3.2 Second step

Using the muon flux obtained from the above studies, the distribution of the vertical stopping position of the muons in the detector was simulated as shown in Figure 5.4. To

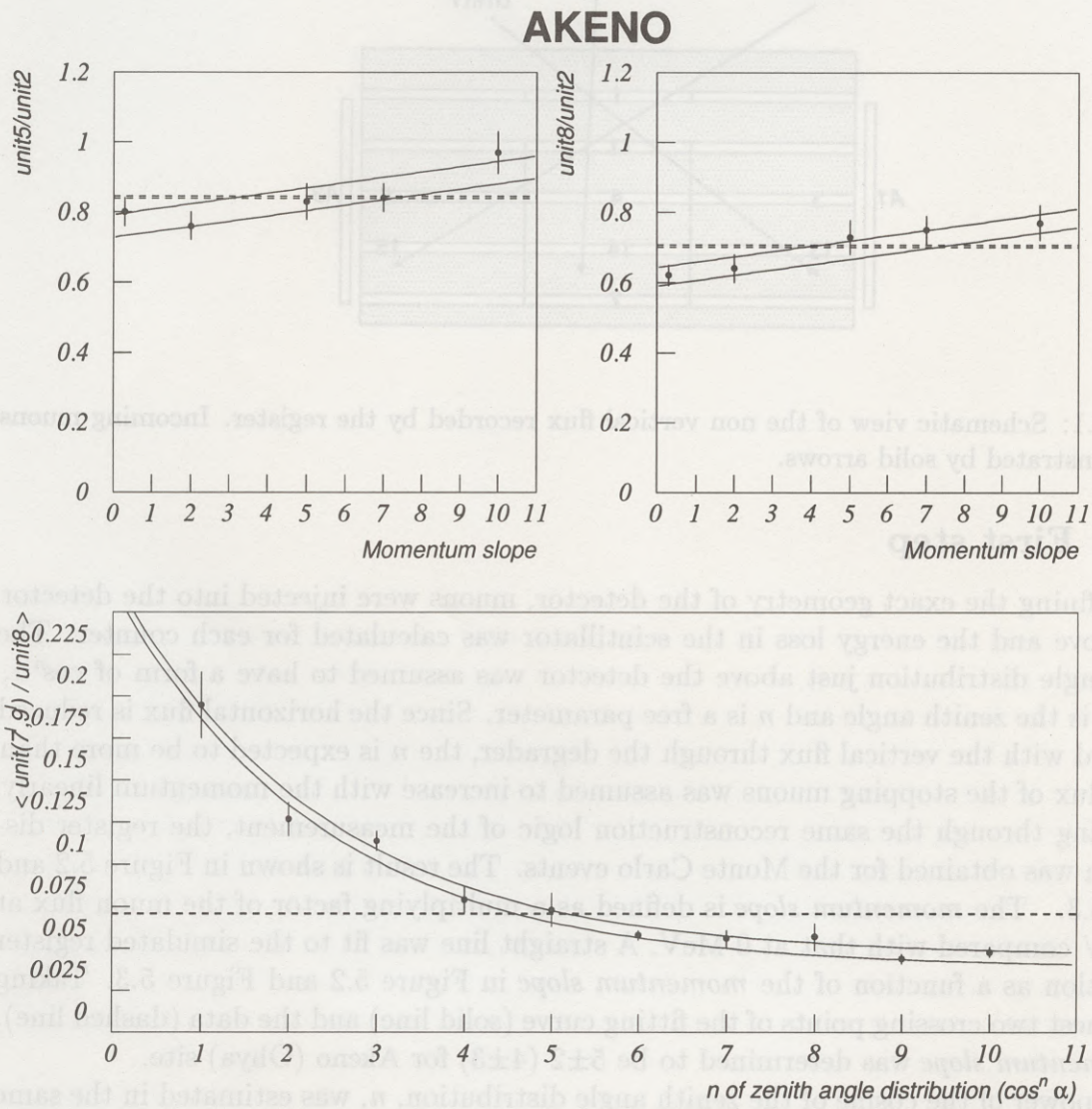

Figure 5.2: The result of the simulated register distribution together with the observed one at Akeno. The point with an error bar is the result of the simulation. The scale of the *momentum slope* is defined as a multiplying factor of the muon flux at 500 MeV compared with that at 0 MeV. A straight line was fit to the simulated points of the upper figure and a general exponential curve defined in the text was fit to that of the lower figure. The distance between the two solid lines shows one standard deviation of the fitting function. The observed register distribution at Akeno site is indicated by the dashed horizontal lines. The distance between the two dashed lines shows one standard deviation of the observed data.

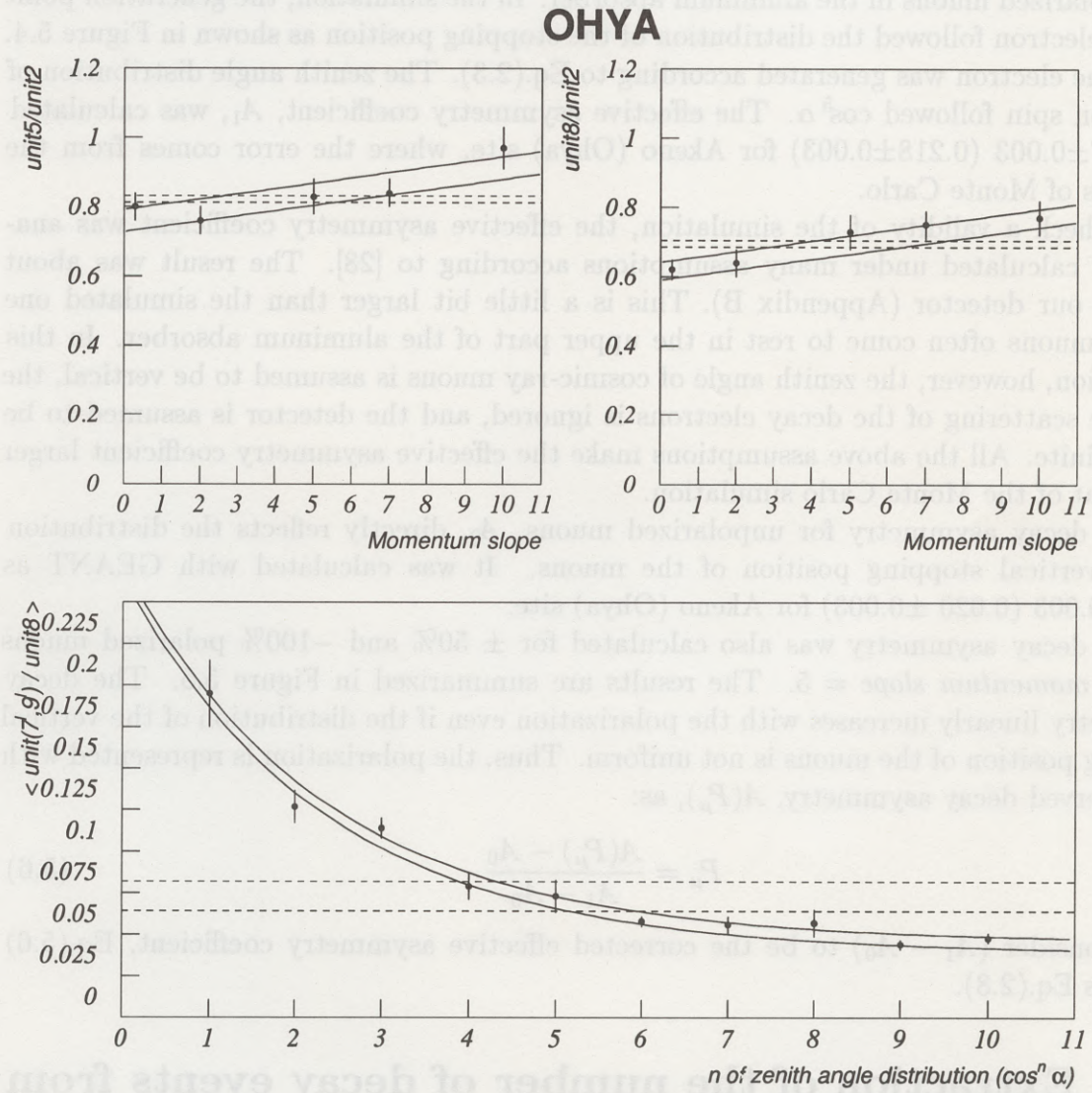

Figure 5.3: The result of the simulated register distribution (point and solid line) together with the observed one (dashed line) at Ohya.

know the distribution of the vertical stopping position is important because the decay asymmetry directly depend on the stopping position as observed in the beam test. Two straight lines, which correspond to the scintillator and the aluminum layer, were fit to the points with some dips corresponding to the detector slack. The fitting result is also shown in Figure 5.4.

The effective asymmetry coefficient was calculated by generating the electrons from 100% polarized muons in the aluminum absorber. In the simulation, the generation point of each electron followed the distribution of the stopping position as shown in Figure 5.4. Then, the electron was generated according to Eq.(2.3). The zenith angle distribution of the muon spin followed $\cos^5\alpha$. The effective asymmetry coefficient, A_1, was calculated as 0.217±0.003 (0.218±0.003) for Akeno (Ohya) site, where the error comes from the statistics of Monte Carlo.

To check a validity of the simulation, the effective asymmetry coefficient was analytically calculated under many assumptions according to [28]. The result was about 0.25 for our detector (Appendix B). This is a little bit larger than the simulated one though muons often come to rest in the upper part of the aluminum absorber. In this calculation, however, the zenith angle of cosmic-ray muons is assumed to be vertical, the multiple scattering of the decay electrons is ignored, and the detector is assumed to be semi-infinite. All the above assumptions make the effective asymmetry coefficient larger than that of the Monte Carlo simulation.

The decay asymmetry for unpolarized muons, A_0, directly reflects the distribution of the vertical stopping position of the muons. It was calculated with GEANT as 0.019±0.003 (0.020 ±0.003) for Akeno (Ohya) site.

The decay asymmetry was also calculated for ± 50% and −100% polarized muons for the *momentum slope* = 5. The results are summarized in Figure 5.5. The decay asymmetry linearly increases with the polarization even if the distribution of the vertical stopping position of the muons is not uniform. Thus, the polarization is represented with the observed decay asymmetry, $A(P_\mu)$, as:

$$P_\mu = \frac{A(P_\mu) - A_0}{A_1 - A_0} \tag{5.6}$$

If we consider $(A_1 - A_0)$ to be the corrected effective asymmetry coefficient, Eq.(5.6) becomes Eq.(2.8).

5.4 Extraction of the number of decay events from TDC data

The number of decay events was extracted from the decay time spectrum recorded by the TDC. The decay time spectra measured at Akeno and Ohya sites are shown in Figure 5.6 and Figure 5.7, respectively. To cancel the up/down asymmetry of the detection efficiency of the counter, the data of the two counter settings were summed. The data of nine *detector unit*s were also summed. The both-hit events were not included in Figure 5.6 and Figure 5.7 to remove the background events such as the accidental cosmic-ray muons and the stopping muons in the upper counter of the *detector unit*.

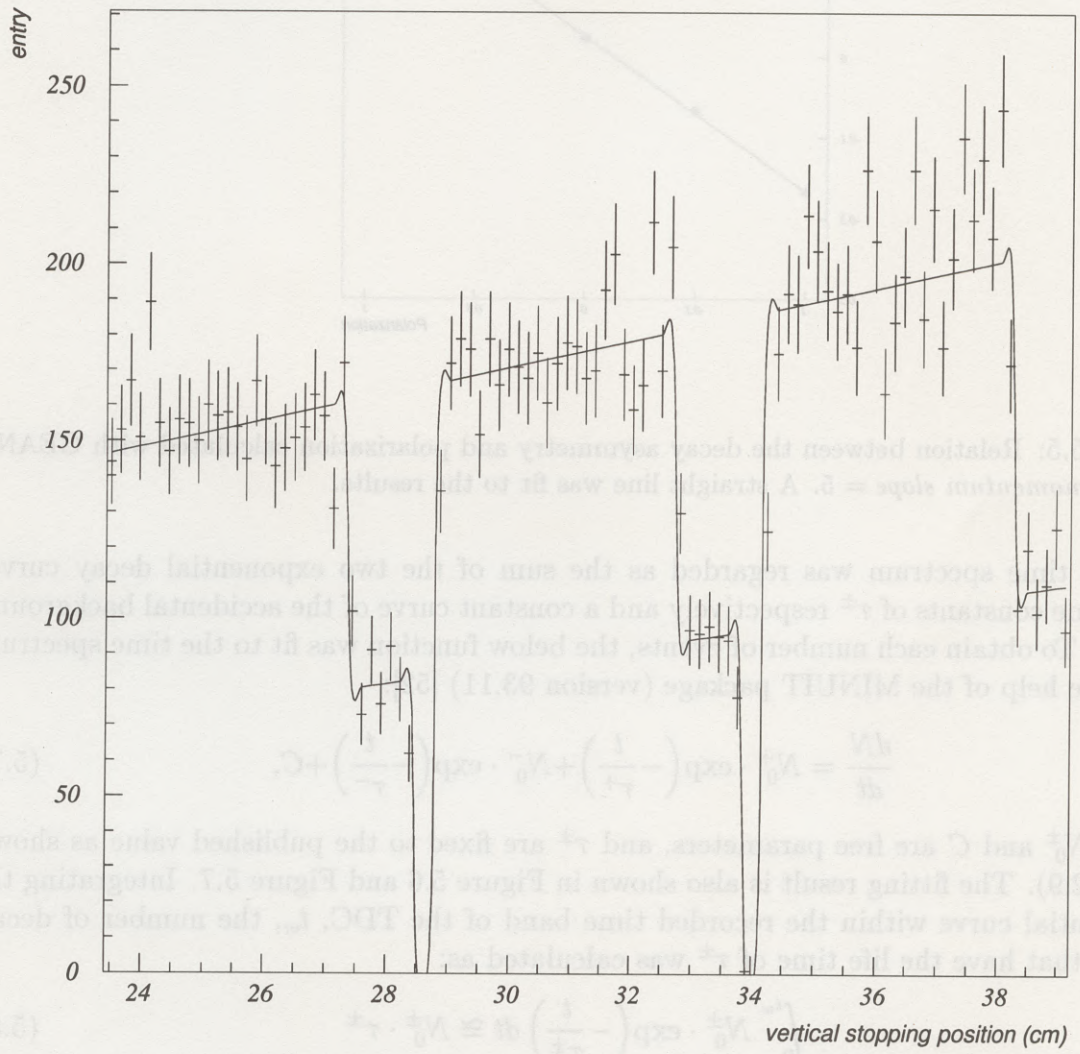

Figure 5.4: The simulated distribution of the vertical stopping position of the muons for the *momentum slope* = 5. The horizontal axis shows a height from the floor of the experimental room. The range of the horizontal axis seen in the figure corresponds to the part of the *detector unit* in the detector. The cross bars are the entries and the solid line shows the fitting result.

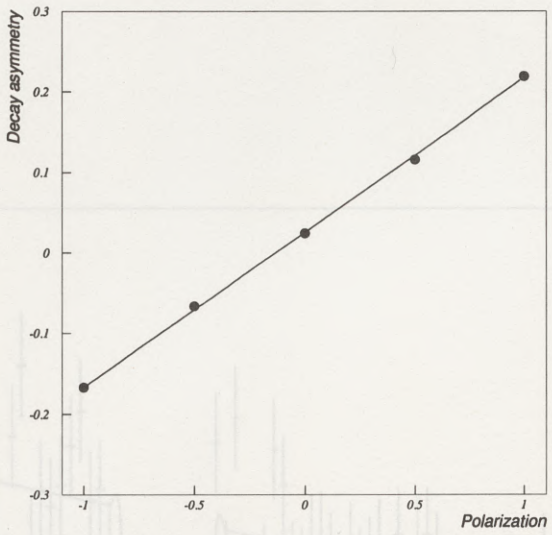

Figure 5.5: Relation between the decay asymmetry and polarization calculated with GEANT for the *momentum slope* = 5. A straight line was fit to the results.

The time spectrum was regarded as the sum of the two exponential decay curves with time constants of $\tau^{\pm}$ respectively and a constant curve of the accidental background events. To obtain each number of events, the below function was fit to the time spectrum with the help of the MINUIT package (version 93.11) [52]:

$$\frac{dN}{dt} = N_0^+ \cdot \exp\left(-\frac{t}{\tau^+}\right) + N_0^- \cdot \exp\left(-\frac{t}{\tau^-}\right) + C, \tag{5.7}$$

where $N_0^{\pm}$ and C are free parameters, and $\tau^{\pm}$ are fixed to the published value as shown in Eq.(2.9). The fitting result is also shown in Figure 5.6 and Figure 5.7. Integrating the exponential curve within the recorded time band of the TDC, t_w, the number of decay muons that have the life time of $\tau^{\pm}$ was calculated as:

$$\int_0^{t_w} N_0^{\pm} \cdot \exp\left(-\frac{t}{\tau^{\pm}}\right) dt \cong N_0^{\pm} \cdot \tau^{\pm} \tag{5.8}$$

In this analysis, the μ^- that comes to rest in the scintillator was assumed to have the same life time of the μ^+ because the life time of those μ^- (2.035 μs [33]) is similar to that of μ^+ (2.197 μs). Thus, the first term of the right part of Eq.(5.7) still includes the background events of the muons that come to rest in the upper scintillator. These background events were removed as described in the next section.

5.5 Calculation of the decay asymmetry

The decay asymmetry was calculated from the fitting results, $N_0^{\pm}$, with some corrections.

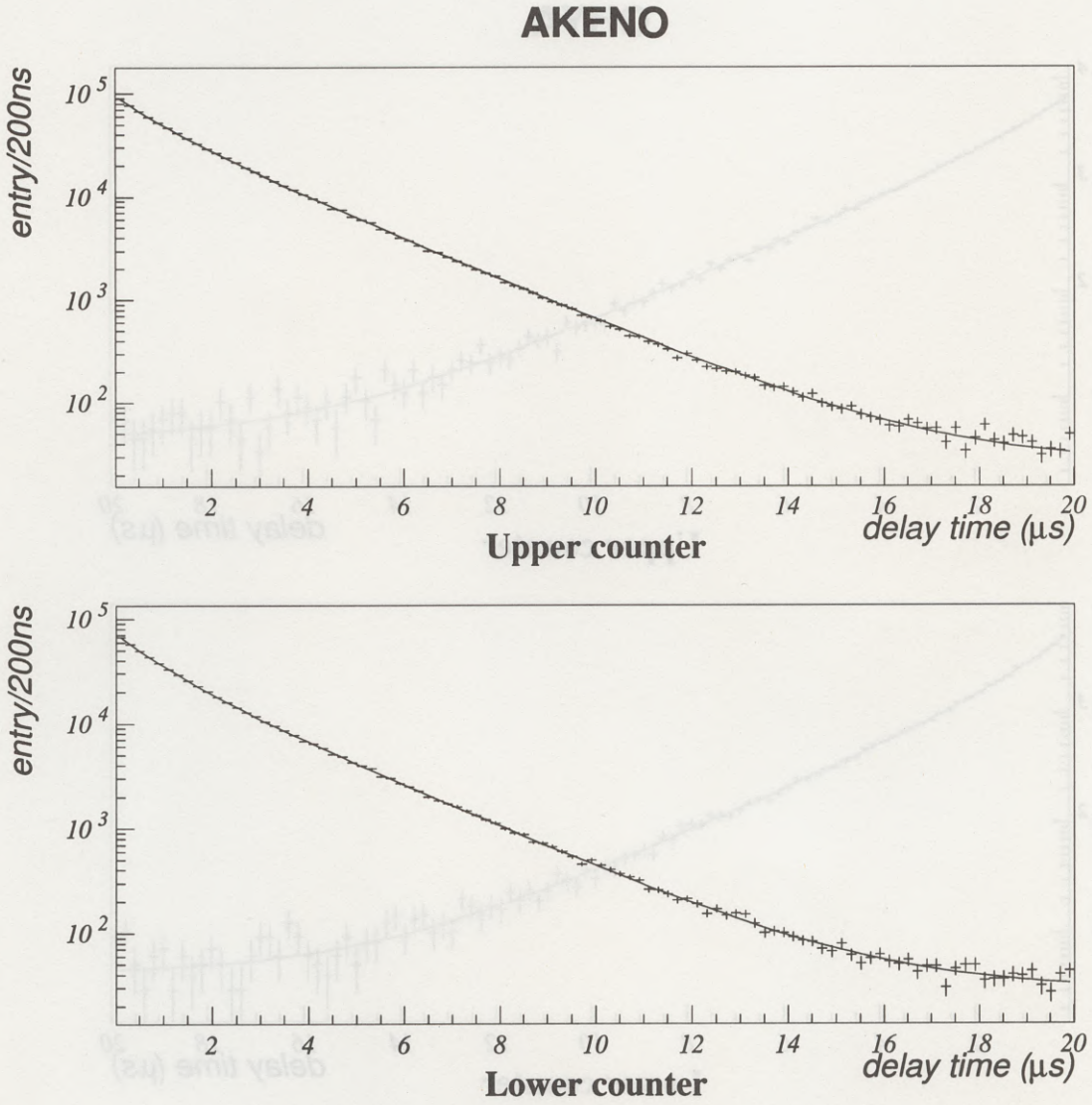

Figure 5.6: Decay time spectrum measured in the upper and lower counters of the *detector unit* at Akeno site. The cross bars are the entries and the solid curve is the fitting result.

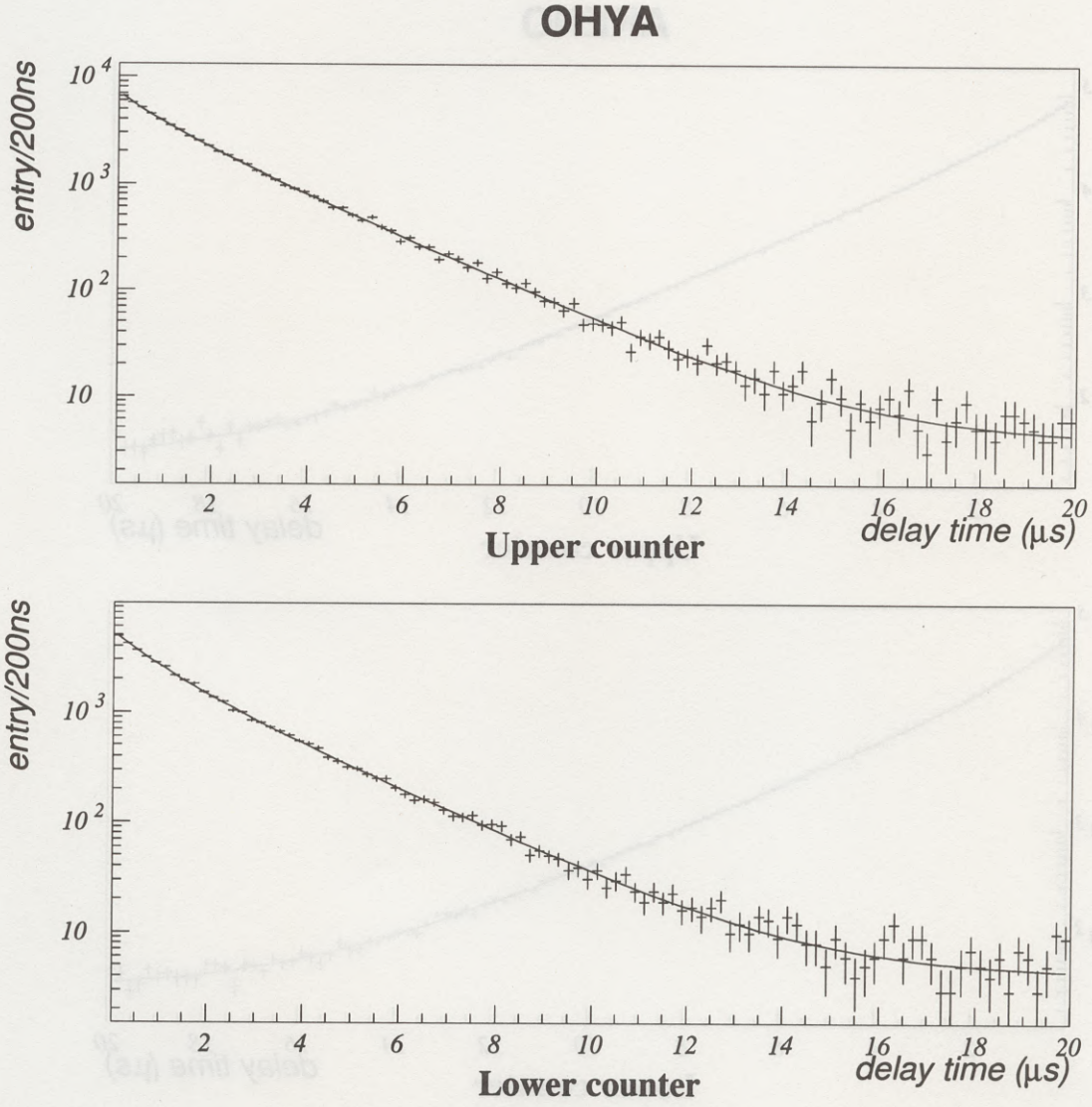

Figure 5.7: Decay time spectrum measured in the upper and lower counters of the *detector unit* at Ohya site.

Using the register information, the set of counters penetrated by the incoming muon is known but the exact stopping position of the muon cannot be determined. The muon that comes to rest in the upper counter becomes a background event, which causes a large decay asymmetry.

The number of decay events obtained from the fitting is represented as:

$$\begin{aligned} U_L &= u^+_{al} + u^+_{sc} + u^-_{sc}, \\ D_L &= d^+_{al} + d^+_{sc} + d^-_{sc}, \\ U_S &= u^-_{al}, \\ D_S &= d^-_{al}, \end{aligned} \tag{5.9}$$

where the left part of Eq.(5.9) denotes the observed number of events directly calculated from fitting results as Eq.(5.8). 'U' denotes the number of the events detected in the upper counter and 'D' denotes that in the lower counter. A lower subscript 'L' denotes the decay event with a long life time ($\equiv \tau^+$) and 'S' denotes that with a short life time ($\equiv \tau^-$). For example, U_L is equal to $N^+_0 \cdot \tau^+$ of the upper counter.

The left part of Eq.(5.9) can be decomposed into the right part of that. 'u (d)' denotes the number of the events detected in the upper (lower) counter. The upper subscript denotes the charge of the muon and the lower subscript denotes the material where the muon decays. 'al' denotes the aluminum and 'sc' denotes the upper scintillator. For example, u^+_{al} denotes the number of the decay electrons emerged from the stopping μ^+ in the aluminum and detected in the upper counter.

Further,

$$\begin{aligned} u^+_{sc} &= N^+_{sc} \cdot \varepsilon_{sc,u} \cdot (1 - \varepsilon_{sc,d}), \\ u^+_{al} &= N^+_{al} \cdot \varepsilon_{al,u}, \\ u^-_{sc} &= N^-_{sc} \cdot \varepsilon_{sc,u} \cdot (1 - \varepsilon_{sc,d}), \\ u^-_{al} &= N^-_{al} \cdot P_{al} \cdot \varepsilon_{al,u}, \\ d^+_{sc} &= N^+_{sc} \cdot \varepsilon_{sc,d} \cdot (1 - \varepsilon_{sc,u}), \\ d^+_{al} &= N^+_{al} \cdot \varepsilon_{al,d}, \\ d^-_{sc} &= N^-_{sc} \cdot \varepsilon_{sc,d} \cdot (1 - \varepsilon_{sc,u}), \\ d^-_{al} &= N^-_{al} \cdot P_{al} \cdot \varepsilon_{al,d}, \end{aligned} \tag{5.10}$$

where 'ε' denotes the detection efficiency and 'N' denotes the number of the stopping muons. For example, 'N^+_{sc}' denotes the number of the μ^+ that come to rest in the upper scintillator and '$\varepsilon_{sc,u}$' denotes the detection efficiency of the upper counter for the decay electron emerged from muon that decays in the upper scintillator. P_{al} (=0.393 [33]) is the decay probability of the stopping μ^- in aluminum. Note that the decay probability of the stopping μ^- in plastic was assumed to be 1. The term, $(1 - \varepsilon)$, is included to remove the both-hit events.

These quantities are connected with each other as:

$$R_{ch} = \frac{N^+_{sc}}{N^-_{sc}} = \frac{N^+_{al}}{N^-_{al}},$$

$$F_{sc} = \frac{N^+_{sc}}{N^+_{sc}+N^+_{al}} = \frac{N^-_{sc}}{N^-_{sc}+N^-_{al}}, \tag{5.11}$$

where R_{ch} (~ 1.25 [18]) is the charge ratio of cosmic-ray muons and F_{sc} is a fraction of the number of the stopping muon in the upper scintillator to the number of the total stopping muon in both scintillator and aluminum. F_{sc} was estimated with GEANT as about 0.120.

The decay asymmetry of the μ^+ is written as:

$$A^+ = \frac{u^+_{al} - d^+_{al}}{u^+_{al} + d^+_{al}}, \tag{5.12}$$

where u^+_{al} and d^+_{al} are obtained from Eq.(5.9), Eq.(5.10), and Eq.(5.11) as:

$$\begin{aligned} u^+_{al} &= U_L - N^+_{sc} \cdot \left(1 + \frac{1}{R_{ch}}\right) \cdot \varepsilon_{sc,u} \cdot (1 - \varepsilon_{sc,d}) \\ d^+_{al} &= D_L - N^+_{sc} \cdot \left(1 + \frac{1}{R_{ch}}\right) \cdot \varepsilon_{sc,d} \cdot (1 - \varepsilon_{sc,u}) \end{aligned} \tag{5.13}$$

The second term of the right part of Eq.(5.13) represents the number of the background events. The number of the stopping μ^+ in the upper scintillator, N^+_{sc}, was estimated as:

$$N^+_{sc} = \frac{N_b}{\left(1 + \frac{1}{R_{ch}}\right) \cdot \varepsilon_{sc,u} \cdot \varepsilon_{sc,d}}, \tag{5.14}$$

where N_b is the observed number of the both-hit events excluding the accidental coincidental events. Figure 5.8 shows the decay time spectrum for the both-hit event for both sites. The below function was fit to the data:

$$\frac{dN}{dt} = (N_0)_b \cdot \exp\left(-\frac{t}{\tau^+}\right) + C_b, \tag{5.15}$$

where $(N_0)_b$ and C_b are free parameters. The number of decay events, N_b, was obtained as $(N_0)_b \cdot \tau^+$.

The detection efficiency $\varepsilon_{sc,u}$ was measured as 0.640 ± 0.007 in the preparatory experiment as described later. The detection efficiency $\varepsilon_{sc,d}$ was estimated with GEANT as 0.076 ± 0.001 under the assumption that the residual polarization of the stopping muons in the plastic scintillator is zero [53].

On the other hand, the decay asymmetry of μ^- is directly connected with the fitting results without any corrections as:

$$A^- = \frac{u^-_{al} - d^-_{al}}{u^-_{al} + d^-_{al}} = \frac{U_S - D_S}{U_S + D_S} \tag{5.16}$$

The measured quantities, U_L, D_L, U_S, D_S, and N_b, are summarized in Table 5.6. The decay asymmetry of the $\mu^\pm$ was calculated as shown in Table 5.6. The simulated one is also shown in this table.

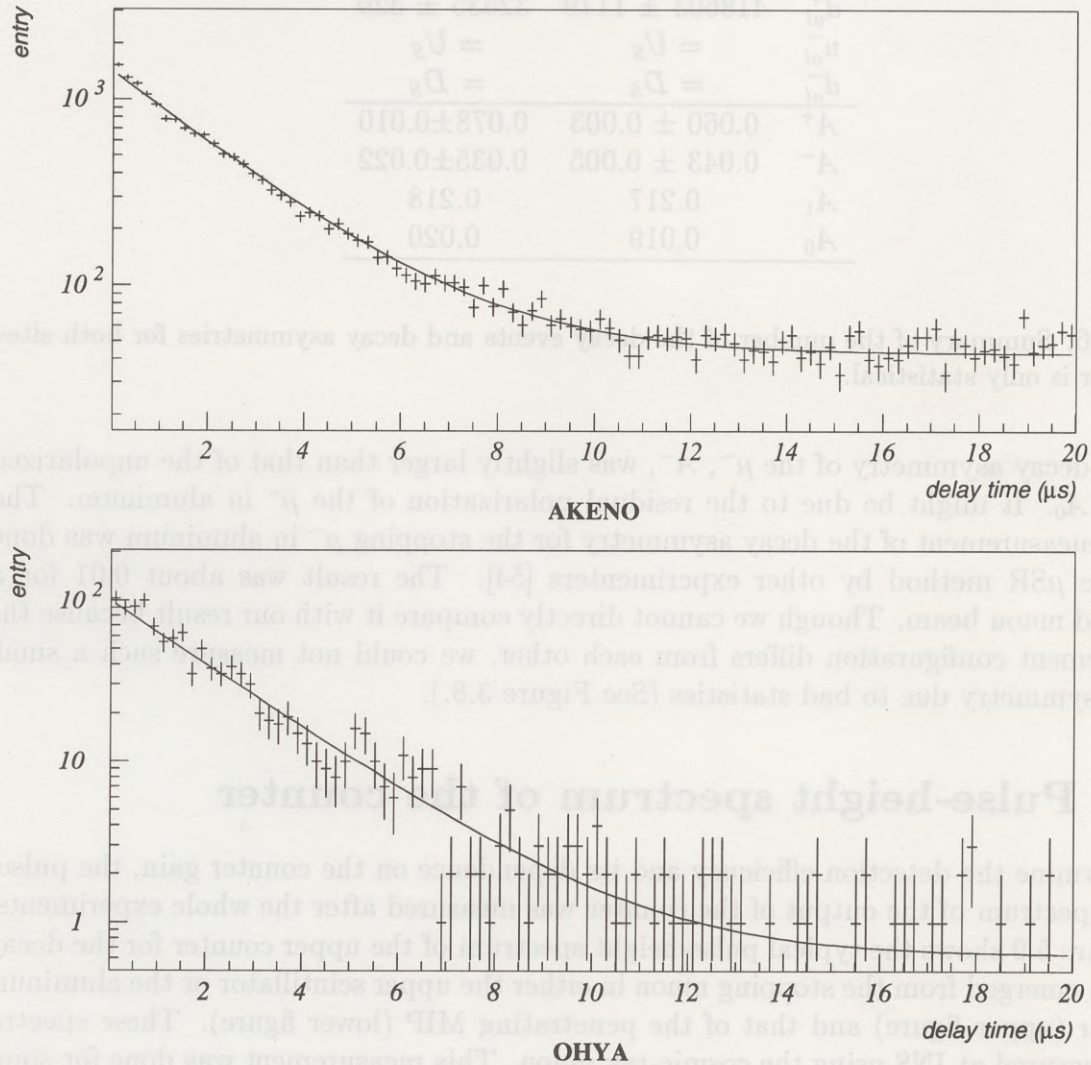

Figure 5.8: The decay time spectrum for the both-hit events. The upper (lower) figure is for Akeno (Ohya) site. The fitting result is also shown in the figure.

	Akeno	Ohya
U_L	654821 ± 1427	51153 ± 399
D_L	427038 ± 1177	33140 ± 328
U_S	157068 ± 1220	10512 ± 337
D_S	144221 ± 1030	9808 ± 283
N_b	14996 ± 135	1076 ± 35
u_{al}^+	472501 ± 2175	38071 ± 583
d_{al}^+	418603 ± 1179	32535 ± 329
u_{al}^-	$= U_S$	$= U_S$
d_{al}^-	$= D_S$	$= D_S$
A^+	0.060 ± 0.003	0.078±0.010
A^-	0.043 ± 0.005	0.035±0.022
A_1	0.217	0.218
A_0	0.019	0.020

Table 5.6: Summary of the number of the decay events and decay asymmetries for both sites. The error is only statistical.

The decay asymmetry of the μ^-, A^-, was slightly larger than that of the unpolarized muons, A_0. It might be due to the residual polarization of the μ^- in aluminum. The precise measurement of the decay asymmetry for the stopping μ^- in aluminum was done with the μSR method by other experimenters [54]. The result was about 0.01 for a polarized muon beam. Though we cannot directly compare it with our result because the measurement configuration differs from each other, we could not measure such a small decay asymmetry due to bad statistics (See Figure 3.8.).

5.6 Pulse-height spectrum of the counter

To determine the detection efficiency and its dependence on the counter gain, the pulse-height spectrum of the output of the counter was measured after the whole experiments.

Figure 5.9 shows the typical pulse-height spectrum of the upper counter for the decay electron emerged from the stopping muon in either the upper scintillator or the aluminum absorber (upper figure) and that of the penetrating MIP (lower figure). These spectra were measured at INS using the cosmic-ray muon. This measurement was done for some counters used in the measurement of the polarization of cosmic-ray muons. The pulse-height was recorded with the FADC. These spectra are the averaged ones for all positions on the scintillator obtained with trigger counters of the same size just above and below the tested counter. Figure 5.9 shows that the detection efficiency of both counters is not affected by the fluctuation of the counter gain in practice. The similar spectra were obtained for the other counters.

The upper spectrum of Figure 5.9 is the weighted sum of a MIP spectrum and a spectrum shown in Figure 5.10. Figure 5.10 shows the pulse-height spectrum of the

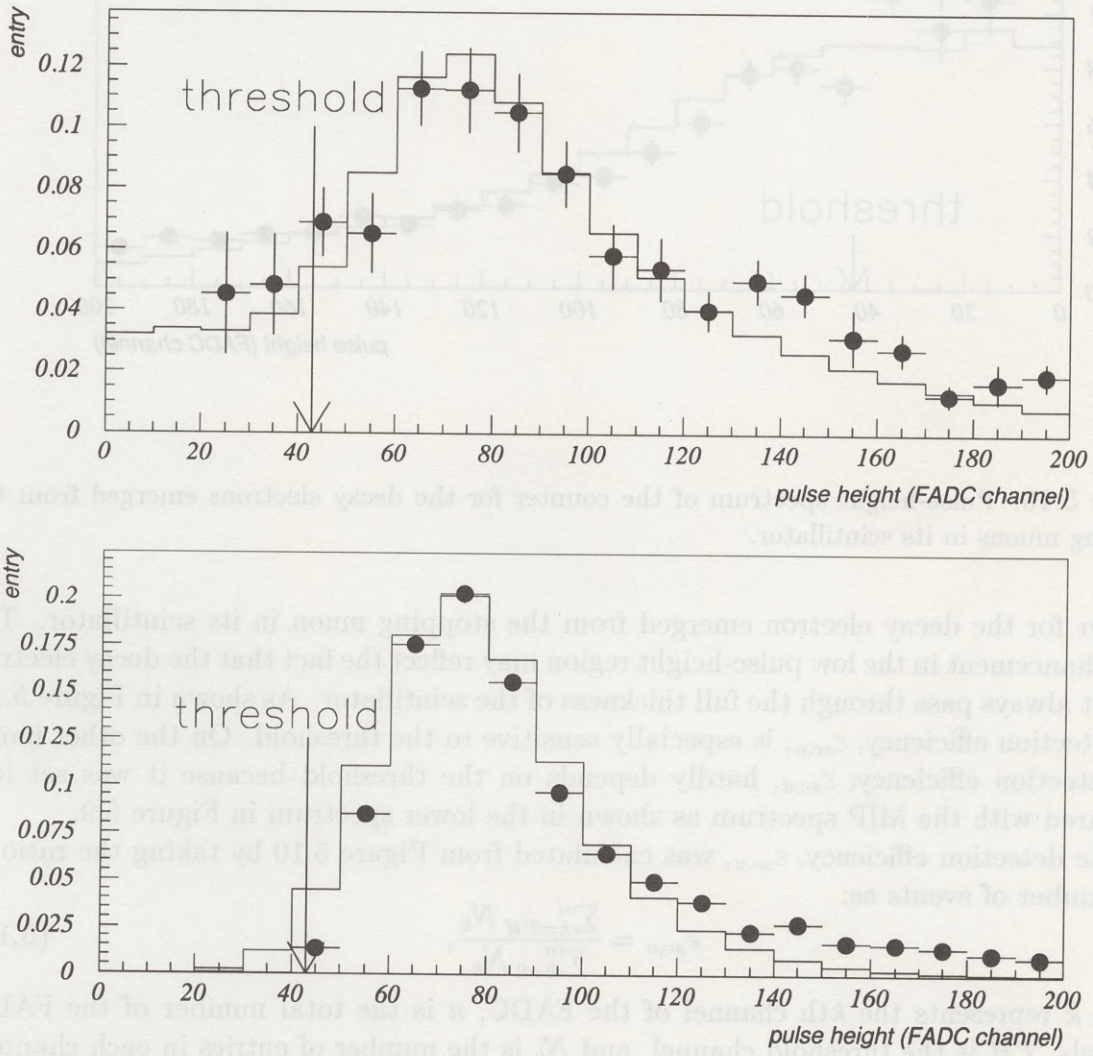

Figure 5.9: Typical pulse-height spectra of the upper counter for the decay electrons emerged from the muons stopped in either the upper scintillator or the aluminum absorber (upper) and that for penetrating MIP's (lower). The points with the error bar are the measured data and the histogram shows the result of the Monte Carlo simulation. The threshold used in this experiment is also shown in the figures. The horizontal scale is adjusted so that the peak pulse-height of the observed MIP spectrum matches with that of the simulated spectrum. Both spectra are normalized to the number of entries.

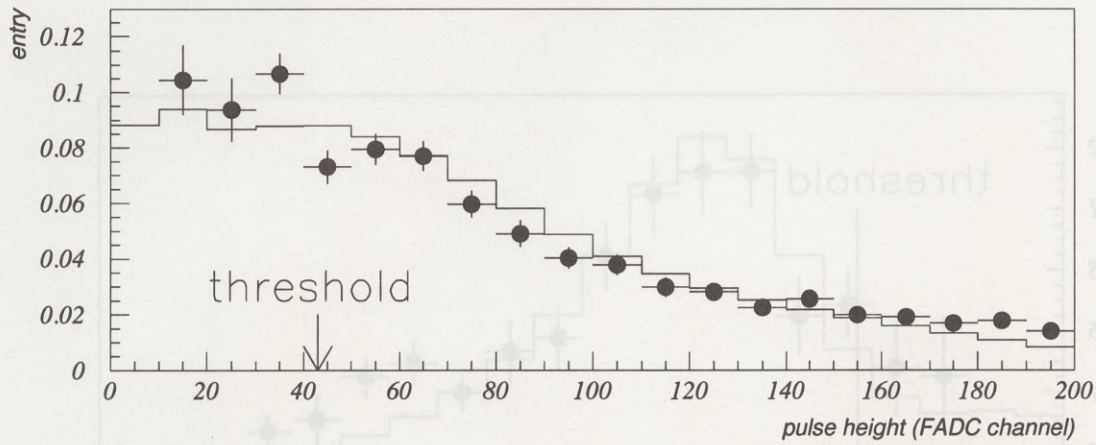

Figure 5.10: Pulse-height spectrum of the counter for the decay electrons emerged from the stopping muons in its scintillator.

counter for the decay electron emerged from the stopping muon in its scintillator. The flat enhancement in the low pulse-height region may reflect the fact that the decay electron did not always pass through the full thickness of the scintillator. As shown in Figure 5.10, the detection efficiency, $\varepsilon_{sc,u}$, is especially sensitive to the threshold. On the other hand, the detection efficiency, $\varepsilon_{sc,d}$, hardly depends on the threshold because it was set low compared with the MIP spectrum as shown in the lower spectrum in Figure 5.9.

The detection efficiency, $\varepsilon_{sc,u}$, was calculated from Figure 5.10 by taking the ratio of the number of events as:

$$\varepsilon_{sc,u} = \frac{\sum_{k=TH}^{n} N_k}{\sum_{k=0}^{n} N_k}, \tag{5.17}$$

where k represents the kth channel of the FADC, n is the total number of the FADC channels, TH is the threshold channel, and N_k is the number of entries in each channel. It was calculated as 0.640±0.007, where the error comes from the statistics of the entry.

5.7 Estimation of depolarization above and in the detector

The depolarization of the stopping muon in the aluminum absorber was measured in the beam test. However, the depolarization occurring above the detector has not been evaluated yet.

The depolarization in matter except at the very end of the range is caused by Coulomb

	Atmosphere	Degrader
x [g/cm^2]	1000	478 (5940)
X_0 [g/cm^2]	37	26.7 (26.7)
p_i [MeV/c]	3×10^3 (1.6×10^4)	1×10^3 (1.4×10^4)
p_f [MeV/c]	1×10^3 (1.4×10^4)	$\sim$200 ($\sim$200)

Table 5.7: Summary of the parameters about the atmosphere and degrader for Akeno (Ohya) sites.

scattering as [3]:

$$\Delta P_{coulomb} = \frac{E_s^2}{X_0}\int_{p_f}^{p_i}\left(\frac{3}{2}-\frac{m_\mu\beta}{p}\right)\frac{dp}{\beta^2p^2(-dp/dx)}, \tag{5.18}$$

where p (β) is the momentum (velocity) of the muon, m_μ is the mass of the muon, X_0 is the radiation length of matter, p_i (p_f) is the initial (final) momentum of the muon, x is thickness of matter, and E_s ($\sim$21 MeV) is the characteristic energy for the multiple scattering:

$$E_s = \sqrt{\frac{4\pi}{\alpha}}\cdot m_e\cdot c^2, \tag{5.19}$$

where m_e is the electron mass and α is 1/137. These parameters for both the atmosphere and degrader are summarized in Table 5.7. The depolarization in the atmosphere was calculated as 0.6 (0.9×10^{-2})% for Akeno (Ohya) sites. The difference of the results between both sites comes from the difference of the muon momentum. When both $-\beta^2(dp/dx)$ and $-\beta(dp/dx)$ are constant and p_f is negligible compared with p_i, the integral in Eq.(5.18) is carried out as:

$$\Delta P_{coulomb} \cong \frac{3}{2}\cdot\frac{E_s^2}{p_i\cdot p_f}\cdot\left(1-\frac{m_\mu}{3p_f}\right)\cdot\frac{x}{X_0} \tag{5.20}$$

Since p_f, X_0, and x/p_i are the same for both sites, the depolarization is independent of the thickness of the degrader. The depolarization in the degrader (2m thick concrete for Akeno site and 33m thick Ohya-stone for Ohya site) was calculated as about 5% for both sites. In summary the depolarization above the detector, $\Delta P_{coulomb}$, was about 5% for both sites.

The spin-relaxation of the stopping μ^+ in the aluminum absorber reduces the polarization. The depolarization due to the spin-relaxation, ΔP_{relax}, is calculated with Eq.(3.10). Substituting t_d=0.2 μs, t_w=20 μs, T=53 μs, and τ^+=2.2 μs in this equation, ΔP_{relax} becomes about 4% for both sites.

5.8 Systematic error study

Systematic errors on the polarization are summarized in Table 5.8. The procedure of the estimation of each systematic error is described below.

Error source	Absolute error
Uncertainty of momentum distribution of muon flux	± 0.011 (± 0.017)
Uncertainty of angle distribution of muon flux	± 0.005 (± 0.012)
Uncertainty of depolarization of μ^+ in degrader	± 0.004
Uncertainty of counter threshold	± 0.012
Uncertainty of counter gain	± 0.038
Statistical error of $\varepsilon_{sc,u}$ measurement	± 0.016
Uncertainty of depolarization of μ^+ in aluminum	± 0.005
Uncertainty of charge ratio of muon flux	± 0.047
Statistics of Monte Carlo	± 0.027
Total (quadratic sum)	± 0.070 (± 0.072)

Table 5.8: Summary of the systematic errors for Akeno (Ohya) sites. If the error is the same for both sites, the error of Ohya is not shown.

5.8.1 Uncertainty of the momentum distribution of the muon flux

As often stated till now, the decay asymmetry reflects the vertical stopping position of the muon in the aluminum absorber. The *momentum slope* was measured as 5 ± 2 (4 ± 3) for Akeno (Ohya) site. The systematic error on the simulated decay asymmetries, A_0 and A_1, due to the uncertainty of the *momentum slope* was estimated with GEANT as ± 0.002 (± 0.003) for Akeno (Ohya) site. Consequently, the systematic error on the polarization was calculated with Eq.(5.6) as ± 0.011 (± 0.017). Note that the uncertainty of the *momentum slope* affects both A_0 and A_1 by the same amount and does not affect the corrected effective asymmetry coefficient $(A_1 - A_0)$.

The detection efficiencies, $\varepsilon_{sc,u}$ and $\varepsilon_{sc,d}$, were not affected by this source of error according to the GEANT simulation.

5.8.2 Uncertainty of the angle distribution of the muon flux

The zenith angle distribution of the muon flux was measured to be $\cos^{5.0\pm 0.5}\alpha$ ($\cos^{5\pm 1}\alpha$) for Akeno (Ohya) site. The error of the power of the cosine causes the uncertainty on the simulated decay asymmetry, A_1, as ± 0.004 (± 0.007) for Akeno (Ohya) site. Consequently, the systematic error on the polarization becomes ± 0.005 (± 0.012) for Akeno (Ohya) site. Since the angle distribution of the decay electron from the unpolarized muon is uniform, both the decay asymmetry, A_0, and the detection efficiencies, $\varepsilon_{sc,u}$ and $\varepsilon_{sc,d}$, are not affected by the uncertainty of the zenith angle distribution.

The cutoff rigidity at Japan, whose magnetic latitude is about 25 °N, is about 10 GeV [1]. Thus, the east-west effect at Ohya is almost negligible. In fact the counting rate among the anticounters ($S3$-$S6$ in Table 5.2) was almost symmetric at Ohya. On the other hand, the counting rate at Akeno was asymmetric beyond the statistical error. The counting rate of $S3$ ($A0$) was much larger than that of $S5$ ($A2$). The anticounter $A0$

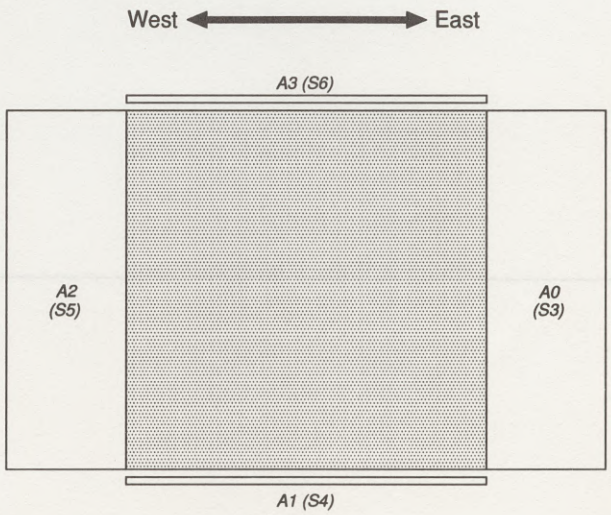

Figure 5.11: Top view of the detector at Akeno site. The anticounter $A0$ was placed toward the about east direction and $A2$ was toward the about west direction.

was placed toward the east and $A2$ was toward the west as shown in Figure 5.11. Thus, the asymmetry might be due to the east-west effect. However, quantitative estimation of the east-west effect on the polarization is difficult due to following reasons:

- The asymmetry detected by anticounters was for all muons with the momentum beyond the lower limit of the energy and was not for the stopping muon.
- The anticounter setting was not geometrically symmetric for the vertical direction though the setting was drawn symmetrically in Figure 2.2. The height of $A0$ differs from that of $A2$ by a few cm.
- The non vertical distribution of the register such like *unit7'/unit8* (See Figure 5.1.) could not be used for the estimation in this detector setting because all counters except anticounters lay along the east-west direction.

The east-west effect on the effective asymmetry coefficient, A_1, was estimated with Monte Carlo simulation. If deflection of the trajectory of the primary cosmic-ray is included, the zenith angle, α, may be replaced with $\alpha + \psi$ (or $\alpha - \psi$) for east (or west) direction for positive muon, where ψ is the deflection angle [55]. In this case, a center axis of the muon arrival direction is tilted toward west with respect to the vertical direction, which may make the A_1 smaller than the non tilted case.

Figure 5.12 shows the azimuth angle distribution of positive cosmic-ray muons of energies of 1 GeV calculated by Honda [56]. The azimuthal asymmetry of the muon flux due to the east-west effect was about 6%. On the other hand, the zenith angle distribution was independent of the azimuth angle.

The A_1 was calculated with Monte Carlo simulation in which the spin direction was determined according to the flux of Honda [56]. The calculated A_1 including the east-west

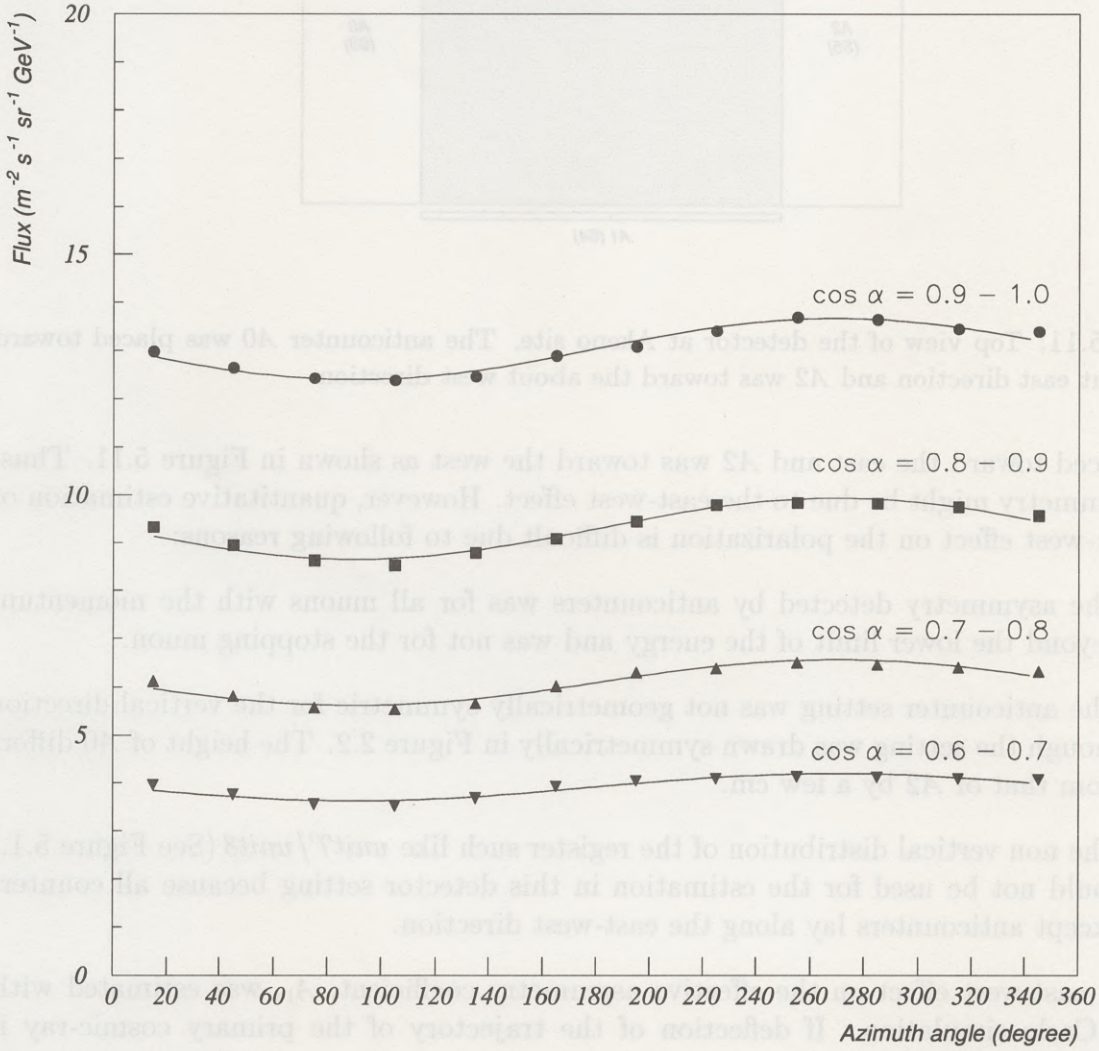

Figure 5.12: Simulated azimuth angle distribution of positive cosmic-ray muons of energies of 1 GeV for some zenith angle regions. The azimuth angle is defined from south direction anticlockwise. Sine curve (solid line) was fit to the data.

effect did not differ from that neglecting the east-west effect within the statistical error of Monte Carlo.

Thus, the zenith angle distribution of the cosmic-ray muon flux was assumed to be symmetric and the azimuth angle distribution was assumed to be uniform in this paper.

5.8.3 Uncertainty of depolarization of μ^+ in the degrader

The depolarization of the μ^+ during the penetration through the atmosphere and degrader was calculated with Eq.(5.18). Since the absolute value of the depolarization in the atmosphere is substantially smaller than that in the degrader, only the depolarization in the degrader is considered here.

The initial momentum of the cosmic-ray muon, p_i, has a range of about 20% around the mean momentum because of the zenith angle distribution of $\cos^5\alpha$. The final momentum, p_f, has a range corresponding to the stopping range of the detector as (200±50) MeV. Consequently, the depolarization of μ^+ above the detector $\Delta P_{coulomb}$ was calculated as (5±1)%. The error of the depolarization causes the systematic error on the polarization as ±0.004.

5.8.4 Uncertainty of the counter threshold

As described before, the detection efficiency, $\varepsilon_{sc,u}$, depends on the counter threshold. It is an important parameter to estimate the number of the background events as shown in Eq.(5.13) and Eq.(5.14).

The threshold was calibrated as follows. The pulse-height spectrum of the output of the counter for the MIP was measured with the ADC. In the off-line analysis, the detection efficiency was calculated from this ADC spectrum as a function of the threshold (ADC channel). Using the same experimental setup of the above measurement, the detection efficiency for the MIP was also measured with a scaler by changing the threshold (mV) of the discriminator. Comparing the threshold dependence of the detection efficiency for both measurements, the conversion coefficient between the discriminator and the ADC was obtained as 0.820±0.004 (mV/ADC channel).

The setting accuracy of the threshold of the discriminator was about 1% during the measurement.

The uncertainty of $\varepsilon_{sc,u}$ due to the uncertainty of the threshold was estimated as ±0.005. Consequently, the systematic error on the polarization becomes ±0.012.

5.8.5 Uncertainty of the counter gain

As described in the detector section, the supply voltage of each counter was set as equalizing each gain to a standard gain. The gain was measured as the mean pulse-height for the MIP. The mean pulse-height was obtained by fitting the peak of the spectrum with a Gaussian function. The fitting error on the mean peak was about 1%, which becomes an uncertainty of the gain.

Each counter has the position dependence of the attenuation of the scintillation light. The character of the position dependence was not the same for all counters. Since the

gain was adjusted using the penetrating MIP at one point on the scintillator (center), it was deviated from the standard gain for some counters. The different character of the attenuation of the scintillation light for each counter causes the difference of the counter gain. The average of the gain, G, was 67.5±1.4 (ADC channel), where the error came from the difference of the attenuation character among the counters. This error was treated as the systematic error.

The temperature coefficient of the counter gain was measured to be about $-0.3\%/°C$. As described in Chapter 4, the room temperature of each experimental site was very stable during the measurement. The difference of the room temperature between each experimental site was several °C at most, which causes the uncertainty of the gain as about 2% at most.

The long-term stability of R580 (PMT) was measured by T.Ishii et al. [57] for about five thousand tubes used in the ZEUS experiment. In their measurement the gain of R580 was stable for two years within ±2%. Using the real data taken in the polarization measurement, the long-term stability of the counter gain during our measurement was investigated in the off-line analysis. Figure 5.13 shows the time dependence of a ratio of the number of the events detected in the upper counter to that in the lower counter for both experimental sites. This ratio is sensitive to the counter gain, since only the upper counter has some low pulse-height hits. A straight line was fit to data of each detector *Setting*. The slopes of each fitting were consistent with zero within the fitting error, which proves the stability of the counter gain during the measurement. The last two points around the 50th day of Akeno site do not mean the deterioration of the counter gain because the ratio of Ohya site never goes down in totally.

In summary, the uncertainty of the detection efficiency, $\varepsilon_{sc,u}$, was estimated as ±0.017. Consequently, the systematic error on the polarization becomes ±0.038.

5.8.6 Statistical error of the $\varepsilon_{sc,u}$ measurement

The detection efficiency, $\varepsilon_{sc,u}$, was measured as 0.640±0.007, where the error comes from the statistics of the $\varepsilon_{sc,u}$ measurement. Consequently, the systematic error on the polarization becomes ±0.016.

5.8.7 Uncertainty of depolarization of μ^+ in aluminum

The depolarization of the stopping μ^+ in aluminum is calculated with Eq.(3.10). Taking into account the measurement error of the spin-relaxation time T, the depolarization ΔP_{relax} was calculated as (4±2)%. The error of the depolarization causes the systematic error on the polarization as ±0.005.

5.8.8 Uncertainty of the charge ratio of the muon flux

According to [18], the charge ratio of the cosmic-ray muons for the vertical direction is 1.25±0.04. The systematic error on the polarization was calculated with Eq.(5.13) as ±0.047.

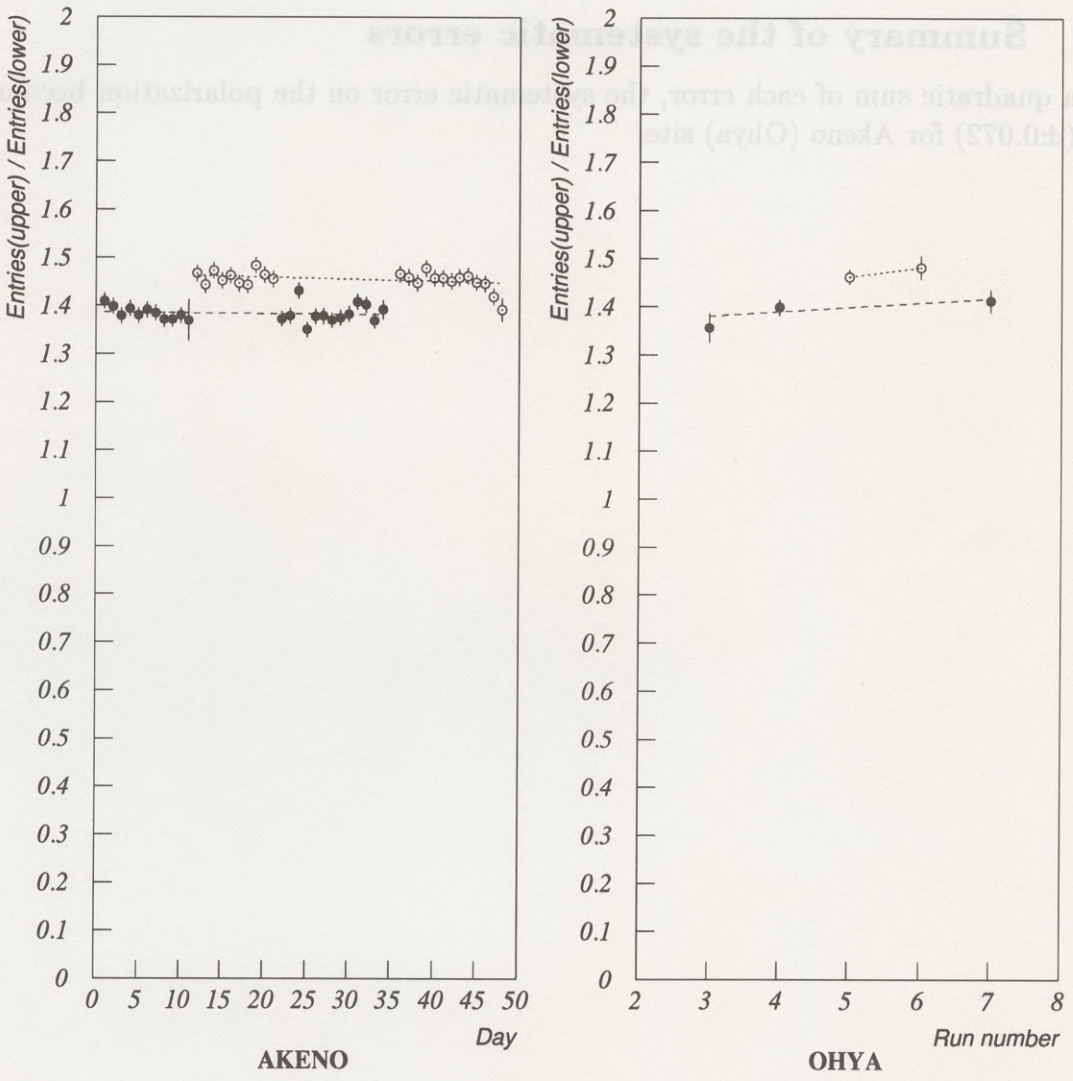

Figure 5.13: The time dependence of the ratio of the number of the events detected in the upper counter to that in the lower counter for both experimental sites. For Ohya site, the horizontal axis is the run number as shown in Table 5.1. The full (open) circles are for the detector *Setting 1* (*Setting 2*). A straight line was fit to data of each *Setting*. The broken (dotted) line is for the *Setting 1 (2)*.

5.8.9 Statistics of the Monte Carlo calculation

Statistical error of the simulated quantities, A_0, A_1, and $\varepsilon_{sc,d}$, were ± 0.003, ± 0.003, and ± 0.001, respectively. The systematic errors on the polarization were estimated as ± 0.014, ± 0.004, and ± 0.023, respectively. Taking the quadratic sum, the systematic error on the polarization becomes ± 0.027.

5.8.10 Summary of the systematic errors

Taking a quadratic sum of each error, the systematic error on the polarization becomes ± 0.070 (± 0.072) for Akeno (Ohya) site.

Chapter 6

Results

The spin-polarization of cosmic-ray muons at production was calculated according to Eq.(5.6) with a correction of the depolarization as:

$$P_\mu = \frac{A^+ - A_0}{A_1 - A_0} \cdot \frac{1}{1 - \Delta P_{coulomb}} \cdot \frac{1}{1 - \Delta P_{relax}}, \tag{6.1}$$

where A^+ is the observed decay asymmetry for μ^+, A_1 (A_0) is the calculated decay asymmetry for 100 (0)% polarized muons according to the Monte Carlo simulation, and $\Delta P_{coulomb}$ (ΔP_{relax}) is the depolarization above (in) the detector. The results are:

$$P_\mu = \begin{cases} 0.227 \pm 0.017\ (stat) \pm 0.070\ (syst) & \text{at Akeno site (}\sim\text{1 GeV)} \\ 0.327 \pm 0.056\ (stat) \pm 0.072\ (syst) & \text{at Ohya site (}\sim\text{14 GeV)} \end{cases}$$

Figure 6.1 shows these results together with those of previous experiments.

Theoretical expectations of the polarization are also shown in Figure 6.1. The dashed lines are the expected polarizations when all muons come exclusively from pions ($\equiv P_\pi$) and kaons ($\equiv P_K$), respectively. In this calculation α was assumed to be 2.65 above 6 GeV and was assumed to fall smoothly to 1.93 at 1 GeV according to [4].

In recent Monte Carlo simulations of the air shower, the K/π ratio is taken to be about 0.1, based on accelerator experiments [58, 59, 60] in the momentum region of the present experiments. The expected value of the polarization ($\equiv P_{ex}$) for a given K/π ratio ($\equiv R$) is given as [5]:

$$P_{ex} = \frac{a \cdot P_\pi + R \cdot P_K}{a + R} \tag{6.2}$$

When the production spectrum of charged and neutral kaons is equal, a becomes 1.494 [5]. The dotted line in Figure 6.1 is the expected polarization for K/π = 0.1. Our results for both experimental sites support this expectation.

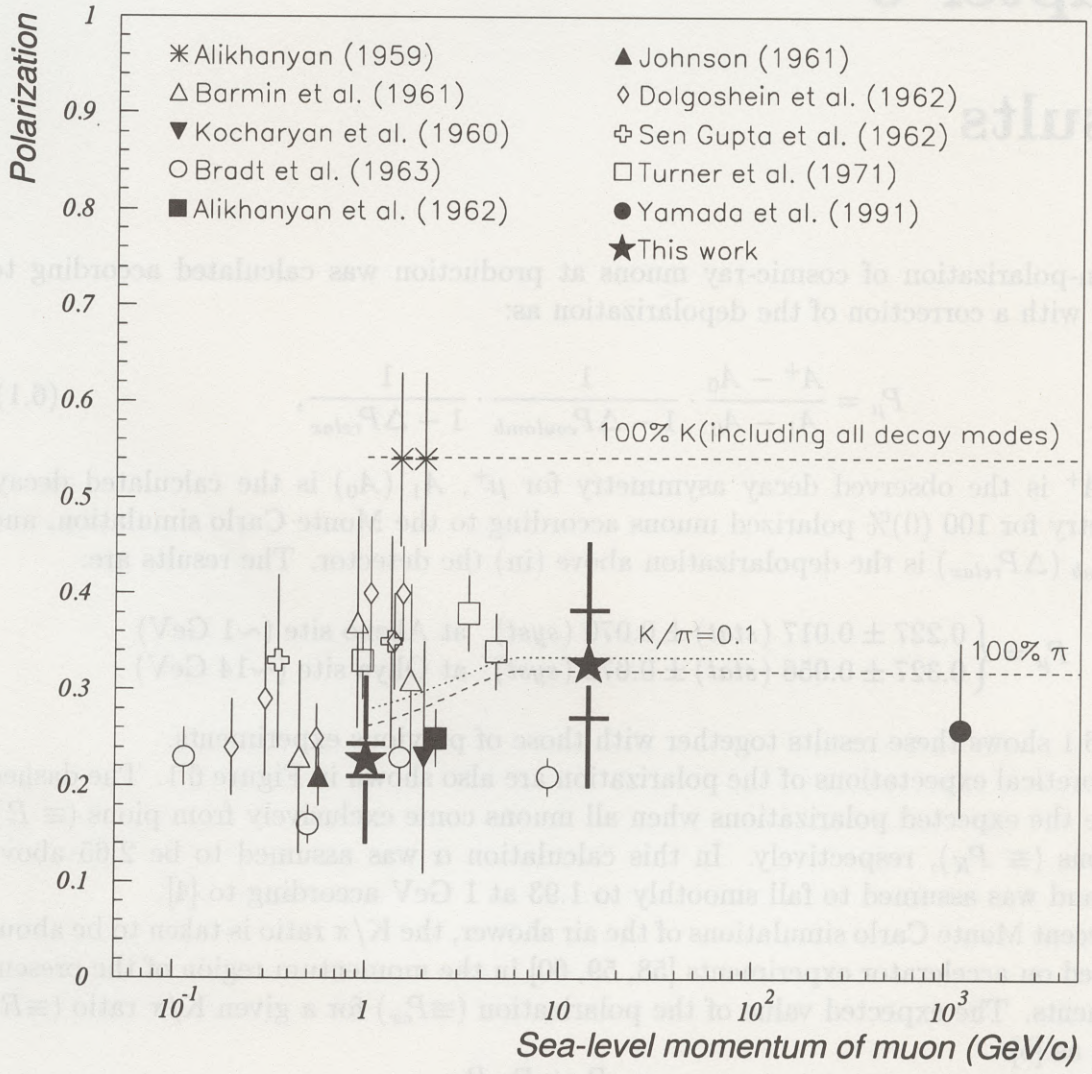

Figure 6.1: Results of the measurement of the spin-polarization of cosmic-ray muons together with those of previous experiments. The full stars are the results of this work. The error bars for this work is a linear sum of the statistical (up to the horizontal short bar) and the systematic error. The theoretical expectations for the parent kaons (~0.54) or pions (~0.32) are also plotted as dashed lines. The theoretical expectations for K/π=0.1 is also shown by a dotted line.

Chapter 7
Discussion

7.1 Comparison with previous experiments

We have measured the spin-polarization of cosmic-ray muons using nearly the same experimental method as the previous experiments. Advantages of this experiment are summarized as follows:

- The detector was calibrated with a polarized muon beam. The observed decay asymmetry for the *detector unit* in the beam test was consistent with that calculated by a Monte Carlo simulation. The depolarization of μ^- in the aluminum absorber was confirmed and the spin-relaxation time of μ^+ was measured with the μSR method. We also measured the life time of $\mu^\pm$. In the previous measurements the detector was not calibrated with a test beam except for the experiment of Turner et al. [29]. The spin-relaxation time has never been measured by previous experiments.
- The detector was simulated precisely using the GEANT Monte Carlo package, which can deal with physical processes such as the multiple scattering and bremsstrahlung. Also, the precise geometry of the detector can be defined in GEANT. Important parameters of the detector that are necessary to calculate the polarization such as the effective asymmetry coefficient were calculated by GEANT in this experiment. In most of the previous experiments, the effective asymmetry coefficient was analytically calculated under many rough approximations. For example, the detector was assumed to be semi-infinite or the range of the decay electrons in the absorber was assumed to be proportional to the energy. In the latter assumption, the multiple scattering of the decay electrons was ignored. These assumptions cause an overestimation of the effective asymmetry coefficient. Consequently, the polarization was underestimated.
- The decay timing was measured by a TDC in this experiment, which allowed us to take data in a shorter time than the previous experiments because the decay electrons were detected by the delayed coincidence method in the previous experiments. In most of the previous experiments, the timing gate for the electron detection was opened from about one to several μs after the muon trigger. On the other hand, the dead time of the present experiment ($\sim$0.2 μs) is shorter than that of previous

experiments and the recorded time band (~20 μs) of our TDC is about twice as long as that of those experiments. The time resolution of the TDC (5 ns) is better than that of the previous experiments. Using this better timing information, we could statistically distinguish the μ^+ and μ^-.

The result at Akeno (1 GeV) is consistent with that of previous experiments in the same momentum region, i.e., Turner et al. [29], Barmin et al. [22], Sen Gupta et al. [28], and Dolgoshein et al. [27]. The result at Ohya (14 GeV) cannot be directly compared with previous experiments. If we compare it with experiments performed at somewhat lower energies, the result at Ohya is again consistent with Turner [29] and Bradt et al. [24].

In Turner's experiment a beam test was done for their detector. Additionally, both the experimental setting and the method of the data analysis are similar to the present experiment. They used aluminum and plastic scintillator for the absorber and the counter, respectively. The μ^+ and μ^- were statistically distinguished and the μ^- that comes to rest in the upper counter was regarded as μ^+ in their analysis, as in ours. However, a transverse magnetic field was applied to the absorber to measure the amplitude of the spin-precession of μ^+ in Turner's experiment. The advantage of this method is that the decay asymmetry caused by the polarization could be easily distinguished from the instrumental asymmetry. Thus, Turner's experiment becomes a good reference to check the reliability of our measurement. Our results are consistent with Turner's results over a wide momentum region.

The results of Bradt, especially at about 10 GeV, are smaller than expected. In Bradt's analysis both depolarization and the multiple scattering of the decay electrons were not taken into account. This might be the reason that their results were systematically smaller.

In the Kamiokande experiment [30], water was used as the absorber. About 20% of incoming μ^+'s form muonium in pure water at room temperature. The magnetic moment of muonium in water is about 70 times larger than that in aluminum [61]. Though the main tank of the Kamiokande detector was surrounded by coils and geomagnetism was weakened to be about 100mG in water, the muonium formed in water is rotated within the time recorded band of the TDC by the remaining geomagnetism. Thus, estimating the residual polarization in water is difficult [62].

7.2 Effect on the atmospheric neutrino flux

The ratio of the observed to calculated atmospheric neutrino flux, R_ν (defined in Eq.(1.6)), is summarized in Table 7.1 [63]. For the calculation of the atmospheric neutrino flux, the flux of Honda et al. [17] was used in the Kamiokande experiment. The flux of Lee et al. [19] was used in the IMB experiment. The flux of Barr et al. [16] was used in Soudan, Frejus, and NUSEX experiments. The difference of $(R_\nu)_{cal}$ is less than a few percent among these fluxes. Note that the results listed in Table 7.1 have already been corrected for the effect of muon polarization. In their calculation of $(R_\nu)_{cal}$ the polarization of cosmic-ray muons was assumed to be about 33% because the K/π ratio was taken to be about 0.1.

Experiment	$(R_\nu)_{obs}/(R_\nu)_{cal}$
Kamiokande (sub-GeV) [7]	$0.60^{+0.06}_{-0.05}\pm0.05$
Kamiokande (multi-GeV) [8]	$0.57^{+0.08}_{-0.07}\pm0.07$
IMB-3 [9, 10]	$0.54\pm0.05\pm0.12$
Soudan-2 [11]	$0.64\pm0.17\pm0.09$
Frejus [64, 65]	$1.06^{+0.19}_{-0.16}\pm0.15$
NUSEX [66]	$0.99^{+0.35}_{-0.25}$

Table 7.1: Summary of the ratio of the observed to calculated R_ν. The first error is statistical error and the second is the systematic error. For Kamiokande experiments, the data are separated into two classes according to the neutrino energy. The neutrino energy is more (less) than 1.33 GeV in 'multi-GeV' ('sub-GeV') data. For NUSEX data, only the statistical error is shown.

An analytic derivation of the atmospheric neutrino ratio is given below under the assumption that only the two-body decay of the light meson is considered and then all mesons or muons decay [15]:

$$(R_\nu)_{cal} = \frac{F(\alpha,r)_{M\to\mu\to\nu_\mu} + F(\alpha,r)_{M\to\nu_\mu}}{F(\alpha,r)_{M\to\mu\to\nu_e}}, \tag{7.1}$$

where $F(\alpha,r)$ is given as:

$$\begin{aligned} F(\alpha,r)_{M\to\mu\to\nu} &= \frac{1-r^\alpha}{\alpha^2(1-r)}\int_0^1 dx\, x^{\alpha-1}\Big[f_0(x) \\ &\quad -\frac{f_1(x)}{1-r}\Big(1+r-2\frac{\alpha}{\alpha+1}\frac{1-r^{\alpha+1}}{1-r^\alpha}\Big)\Big], \\ F(\alpha,r)_{M\to\nu_\mu} &= \frac{(1-r)^{\alpha-1}}{\alpha}, \end{aligned} \tag{7.2}$$

where the subscript M denotes pion or kaon, $r \equiv m_\mu^2/M^2$, and $f_i(x)$ is given in Table 2.1. Since the muon polarization is opposite for particle and antiparticle and the angular distribution of the decay neutrinos with respect to the spin-polarization is also opposite for particle and antiparticle, the distribution expressed in Eq.(7.1) is the same for neutrinos and antineutrinos. For example, $F(\alpha,r)_{\pi^+\to\mu^+\to\bar{\nu_\mu}}$ is equal to $F(\alpha,r)_{\pi^-\to\mu^-\to\nu_\mu}$.

The flux of the atmospheric ν_μ's that come directly from the decay of the light meson is, of course, unaffected by the muon polarization. Nevertheless, $(R_\nu)_{cal}$ becomes about 16 (32)% less than the one calculated ignoring the muon polarization effect ($f_1(x) \to 0$ in Eq.(7.2)) for two-body decay of the pion (kaon).

We roughly estimate the muon polarization effect on $(R_\nu)_{cal}$ under the assumption that $(R_\nu)_{cal}$ decreases linearly with the polarization. If we take the polarization observed at Akeno (Ohya) sites, $(R_\nu)_{cal}$ becomes smaller than the unpolarized case by about 14 (16)%. On the other hand, if we take the polarization assumed in recent Monte Carlo calculation, $(R_\nu)_{cal}$ decreases by about 16% from the unpolarized case. The estimated effect of the polarization on $(R_\nu)_{cal}$ from our results and that from the recent Monte Carlo calculations

agree within a few percent. Thus, our results hardly modify the results listed in Table 7.1. It means that the anomaly observed by Kamiokande, IMB-3, and Soudan-2 remains, even if the muon polarization is taken into account.

Chapter 8

Conclusion

We have measured the longitudinal spin-polarization of cosmic-ray muons of energies of about 1 GeV and 14 GeV employing a well-calibrated detector.

The polarization was obtained by measuring the up/down decay asymmetry of the muons that came to rest in the high-purity aluminum plate. The detector was calibrated with an artificially produced beam muon of known polarization at the BOOM facility at KEK.

The measurements of the spin-polarization of cosmic-ray muons were done at the Akeno and Ohya observatories of ICRR. The observable lower limit of the sea-level muon momentum was about 1 GeV and 14 GeV for each experimental site, respectively.

Based on about 10^6 decay events taken from May to June at Akeno and about 10^5 decay events taken from July to November at Ohya in 1995, the polarization was found to be 0.227 ± 0.017 (*stat*) $\pm$ 0.070 (*syst*) for 1 GeV and 0.327 ± 0.056 (*stat*) $\pm$ 0.072 (*syst*) for 14 GeV.

The result for 1 GeV is consistent with the previous experiment of Turner et al., which may be the most reliable experiment to date. The result for 14 GeV is the first result around 10 GeV, which is also consistent with that of Turner et al. at lower energies. Our results support the value of polarization assumed in recent Monte Carlo calculations of the air shower. Even if the polarization measured in this experiment is included, the anomaly of the ratio of muon neutrinos to electron neutrinos in the atmospheric neutrino flux observed by Kamiokande, IMB-3, and Soudan-2 detectors still remains.

Appendix A

Derivation of polarization in a boosted frame

According to [67], the polarization is represented by a unit vector $\mathbf{P}$. A transformation property of $\mathbf{P}$ is obtained with the aid of the spin vector that forms a four-pseudevector s_μ (μ=0, 1, 2, and 3). A space component of s_μ, $\mathbf{s}$, coincides with $\mathbf{P}$ if the particle is at rest, but it has a component in the direction of the momentum if it is in motion. Since $\mathbf{s}$ is a pseudevector and $\mathbf{p}$ is a vector, the $\mathbf{p}$ component of $\mathbf{s}$ must be proportional to $(\mathbf{P}\cdot\mathbf{p})\mathbf{p}$. The coefficient may be determined by reference to the equation:

$$s_\mu p^\mu = s_0 E - \mathbf{s}\cdot\mathbf{p} = 0 \tag{A.1}$$

Furthermore, we have the relation:

$$s_\mu s^\mu = s_0^2 - \mathbf{s}^2 = -1 \tag{A.2}$$

because at rest $|\mathbf{s}|$=1 and s_0=0, according to Eq.(A.1). We then have:

$$\mathbf{s} = \mathbf{P} + (\mathbf{P}\cdot\mathbf{p})\mathbf{p}/m(E+m), \tag{A.3}$$

$$s_0 = \mathbf{s}\cdot\mathbf{p}/E = \mathbf{P}\cdot\mathbf{p}/m, \tag{A.4}$$

where m is the mass of the muon.

We distinguish quantities referred to the rest system of a parent meson by an asterisk. $\mathbf{P}^*$ is parallel to $\mathbf{p}^*$. Then Eq.(A.3) is simplified as:

$$\mathbf{s}^* = \mathbf{P}^* E^*/m \tag{A.5}$$

In the laboratory system the parent meson has velocity $\mathbf{u}$, so that $\mathbf{s}^*$ and s_0^* are transformed as:

$$\mathbf{s} = \frac{E^*}{m}\mathbf{P}^* + (\gamma-1)\frac{E^*}{mu^2}(\mathbf{P}^*\cdot\mathbf{u})\mathbf{u} + \gamma\frac{p^*}{m}\mathbf{u}, \tag{A.6}$$

$$s_0 = \gamma\left(\frac{p^*}{m} + \frac{E^*}{m}(\mathbf{u}\cdot\mathbf{P}^*)\right), \tag{A.7}$$

where $\gamma=1/\sqrt{1-u^2}$. What we need is the component of polarization along the momentum $\mathbf{p}$. This is given, with $\mathbf{n}=\mathbf{p}/p$, by:

$$(\mathbf{P}\cdot\mathbf{n}) = s_0\frac{m}{p} = \frac{\gamma m}{p}\left(\frac{p^*}{m}+\frac{E^*}{m}(\mathbf{u}\cdot\mathbf{P}^*)\right) \tag{A.8}$$

Here $(\mathbf{u}\cdot\mathbf{P}^*)$ is equal to the cosine of the angle between $\mathbf{u}$ and $\mathbf{p}^*$. This quantity is determined if one fixes the energy of the muon in the laboratory system:

$$E = \gamma\left(E^*+p^*(\mathbf{u}\cdot\mathbf{P}^*)\right) \tag{A.9}$$

Eliminating $(\mathbf{u}\cdot\mathbf{P}^*)$ in Eq.(A.8) in virtue of Eq.(A.9), we obtain:

$$(\mathbf{P}\cdot\mathbf{n}) = \frac{EE^*}{pp^*}-\frac{\gamma m^2}{pp^*} \tag{A.10}$$

Here γ represents the energy of the parent meson.

Appendix B

Evaluation of the effective asymmetry coefficient

The electrons from μ-e decay at rest have energies ranging from zero to a maximum energy of 53 MeV. The average range of electrons having an initial energy of E_{max} =53 MeV is $R{\sim}22$ g/cm^2 in aluminum [68]. We assume that u_0 is the initial energy of a decay electron in units of the maximum energy E_{max}. The range is equal to the vertical thickness of the stopping plate x_0 in units of the range R corresponding to E_{max}. We divide the flux of decay electrons (J) emerging through a surface (top or bottom) of the plate into two parts (J_1 and J_2). The flux J_1 includes those electrons that have initial energy $u \leq u_0$ and J_2 includes those having initial energy $u \geq u_0$. The total flux emerging through a surface is then

$$J = J_1 + J_2 \tag{B.1}$$

We have evaluated the fluxes J_1 and J_2 of the upward-moving electrons from the decay of muons stopped in a 2.70 g/cm^3×4.0 cm aluminum plate in the following way.

Let $Q(x, \theta, u)$ be the probability that a decay electron of energy u emitted at depth x making an angle θ with the vertical direction (See Figure B.1.) will emerge through the surface. We have represented $Q(x, \theta, u)$ by the following step function assuming a linear relation between the range $r(u)$ and energy u of the decay electron as:

$$Q(x, \theta, u) = \begin{cases} 1 & (x < r(u)\cos\theta) \\ 0 & (x > r(u)\cos\theta) \end{cases} \tag{B.2}$$

For an individual electron included in the flux J_1 the conditions required to be satisfied for its energy u and range $r(u)$ are $u \leq u_0$ and $r \leq x_0$. It can be shown from Figure B.1 that only that fraction of the electrons that have the initial energy $u \leq u_0$ will come out of the plate for which the decay took place within a depth $rcos\theta$. The flux J_1 can be represented by the expression:

$$J_1 = K \int_0^{rcos\theta} dx \int_0^{\pi/2} d\theta \int_0^{u_0} du \, \frac{1}{2} \sin\theta \cdot g(u, \theta, P) \cdot Q(x, \theta, u) \tag{B.3}$$

where K is the constant depending on the number of muons stopped per unit absorber thickness per unit time, and $g(u, \theta, P)$ is the distribution function for the electrons from

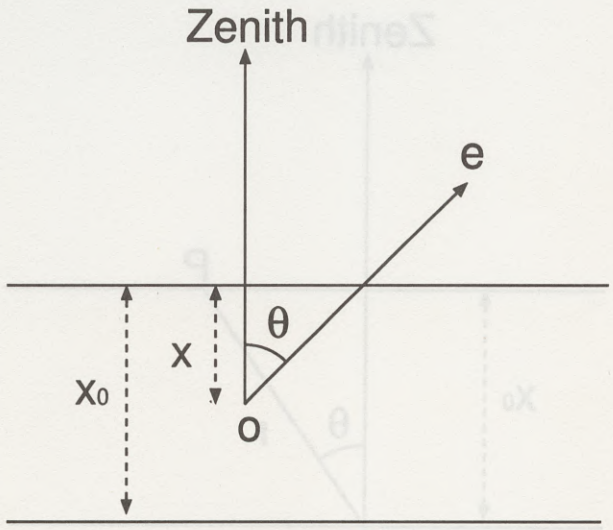

Figure B.1: Emission of an electron at a depth x making an angle θ with the zenith.

the decay of muons with polarization P (See Eq.(2.3)). Then,

$$J_1 = K\Big[-\frac{1}{5}x_0^5 + \frac{3}{8}x_0^4 - \Big(-\frac{2}{15}x_0^5 + \frac{1}{12}x_0^4\Big)P\Big] \tag{B.4}$$

For an individual electron included in the flux J_2 the conditions required to be satisfied for its energy u and range r are $u_0 \leq u \leq 1$ and $x_0 \leq r \leq 1$. We assume that the electrons included in J_2 are coming from two different angular regions, I and II. Region-I includes those electrons ejected within the angular interval

$$0 \leq \theta \leq \cos^{-1}(x_0/r) \tag{B.5}$$

for which $r\cos\theta > x_0$, and region-II include those ejected within the interval

$$\cos^{-1}(x_0/r) \leq \theta \leq \frac{1}{2}\pi \tag{B.6}$$

for which $rcos\theta < x_0$. Figure B.2 shows how the angular interval from 0 to $\pi/2$ is divided into two regions.

For region-I, all electrons of energy $u \geq u_0$ that emitted anywhere in the plate will come out. So

$$\int_0^{x_0} dx\ Q(x,\theta,u) = x_0 \tag{B.7}$$

For region-II, only those electrons of energy $u \geq u_0$ emitted within the depths $rcos\theta < x_0$ will come out. So

$$\int_0^{r\cos\theta} dx\ Q(x,\theta,u) = r\cos\theta \tag{B.8}$$

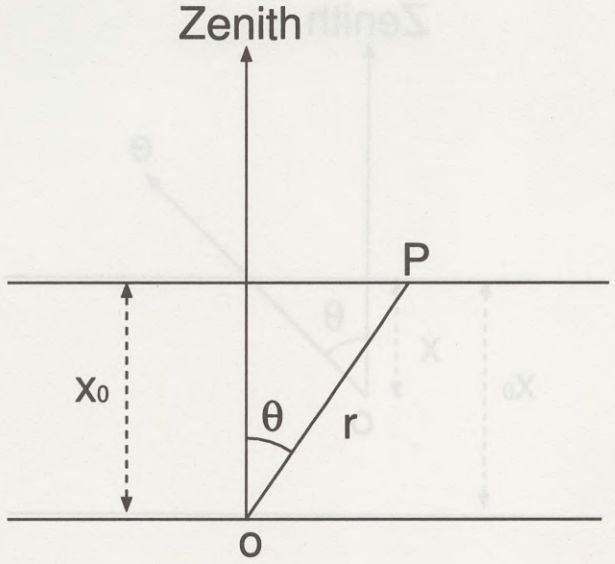

Figure B.2: Schematic view of the two angular regions. Region-I : $0 \leq \theta \leq \cos^{-1}(x_0/r)$, Region-II : $\cos^{-1}(x_0/r) \leq \theta \leq \pi/2$ for electrons $u \geq u_0$ contributing to the flux J_2. OP is the line of division.

The flux J_2 is then given as:

$$\begin{aligned} J_2 &= K\int_{u_0}^{1} du \int_{0}^{\cos^{-1}(x_0/r)} d\theta \, \frac{1}{2}\sin\theta \cdot x_0 \cdot g(u,\theta,P) \\ &\quad + K\int_{u_0}^{1} du \int_{\cos^{-1}(x_0/r)}^{\pi/2} d\theta \, \frac{1}{2}\sin\theta \cdot r\cos\theta \cdot g(u,\theta,P) \\ &= x_0^4\left[\left(\frac{x_0}{6} - \frac{1}{4} - \frac{5}{12x_0^2} + \frac{1}{2x_0^3}\right) - \left(\frac{x_0}{12} - \frac{1}{12x_0^3}\right)P\right] \end{aligned} \tag{B.9}$$

From Eq.(B.4) and Eq.(B.9) we obtain the upward flux as

$$\begin{aligned} J_U &= J_1 + J_2 \\ &= c(1 + F(x_0)P), \end{aligned} \tag{B.10}$$

where c is the constant and $F(x_0)$ is the function of x_0. Similarly we got for the downward flux

$$J_D = c(1 - F(x_0)P) \tag{B.11}$$

Thus, the decay asymmetry was calculated as:

$$\frac{J_U - J_D}{J_U + J_D} = F(x_0) \cdot P \equiv A_1 \cdot P, \tag{B.12}$$

where the effective asymmetry coefficient was calculated as:

$$A_1 = \left(\frac{3}{5}x_0^4 - x_0^3 + 1\right) \Big/ \left(-\frac{2}{5}x_0^4 + \frac{3}{2}x_0^3 - 5x_0 + 6\right) \tag{B.13}$$

Substituting x_0=0.5 in Eq.(B.13), A_1 becomes 0.25.

Acknowledgments

First, I would like to express warm thanks to Prof.S.Yamada for his guidance and encouragement throughout graduate school and for suggesting the theme of this thesis. Without his support and suggestions, I would have never finished this work.

I would like to thank Dr.T.Ishii for his useful discussions on data analysis and on the draft of this thesis.

Prof.K.Tokushuku taught me many things about high energy physics, especially on hardware, throughout graduate school. I thank him very much for his kind encouragement.

In this experiment, I made the detector with a lot of help from INS staffs. Thanks are due to Mr.K.Shiino who taught me many things about electric circuits and other hardware in general not only for this experiment throughout these five years. I also would like to thank Mr.N.Sakamoto for his technical guidance on the construction of the detector.

Dr.I.Fleck checked English of this thesis and gave me useful advices on physics analysis.

I would like to thank Prof.K.Nagamine, Prof.K.Nishiyama, and Dr.S.Sakamoto for their kind support during the beam test at the BOOM facility at KEK. Prof.K.Nagamine gave me a chance to use the BOOM facility many times. I am also indebted to Prof.K.Nishiyama and Dr.S.Sakamoto for their useful advices and help on the μSR measurement.

I would like to thank Prof.M.Nagano, Dr.N.Hayashida, Mr.H.Ohoka, and other Akeno staffs for their hospitality during my stay at Akeno.

I wish to thank Prof.A.Ohashi, Prof.K.Mitsui, and Mr.T.Aoki. Prof. A.Ohashi gave me a chance to use the Ohya underground facility extending the planned time limit. Prof.K.Mitsui and Mr.T.Aoki introduced me to the Ohya facility and made space available for this experiment.

I would like to thank Dr.M.Honda, who calculated the cosmic-ray muon flux which was used to estimate the east-west effect on the present experiment.

Useful discussions about the experiment with Dr.T.Hasegawa, Dr.M.Nakao, Mr.I.Suzuki, and Dr.Y.Yamazaki are acknowledged.

I would like to thank Mr.M.Inuzuka, Mr.K.Umemori, Mr.T.Abe, and Mr.T.Uesugi for their help in carrying out the experiments at INS, Akeno, Ohya and the beam test at KEK.

Finally, I would like to thank my parents for their continuous encouragement and financial support for my studies.

Bibliography

[1] M.Oda, *Cosmic rays*, 1972 (2nd edition), Syokabo, Tokyo.

[2] Review of Particle Properties, Particle Data Group, Phys.Rev., D50 (1994).

[3] S.Hayakawa, Phys.Rev.108,1533(1957).

[4] M.Gardener et al., Proc.Phys.soc.,80,697(1962).

[5] J.L.Osborne, Nuove Cimento 32, 816(1964).

[6] K.S.Hirata *et al.*, Phys.Lett.B205,416(1988).

[7] K.S.Hirata *et al.*, Phys.Lett.B280,146(1992).

[8] Y.Fukuda *et al.*, Phys.Lett.B335,237(1994).

[9] D.Casper *et al.*, Phys.Rev.Lett.66,2561(1991).

[10] R.Becker-Szendy *et al.*, Phys.Rev.D46,3720(1992).

[11] P.Litchfield,for the Soudan-2 Collaboration, Proc.of the International Workshop on ν_μ/ν_e Problem in Atmospheric Neutrinos, Laboratory Nazionali del Gran Sasso, Italy, March 1993: M.C.Goodman,for the Soudan-2 Collaboration, Proceedings of Neutrino '94, International Conference on Neutrino Physics and Astrophysics, Eilat,Israel,May-June 1994.

[12] S.M.Bilenky and B.Pontecorvo, Phys.Rep. 42(1978)225.

[13] S.M.Bilenky and S.T.Petcov, Rev.Mod.Phys.59(1987)671.

[14] L.V.Volkova, Sov.J.Nucl.Phys.37,784(1980).

[15] S.Barr,T.K.Gaisser,P.Lipari and S.Tilav, Phys.Lett.B214,147(1988).

[16] S.Barr,T.K.Gaisser and T.Stanev, Phys.Rev.D39,3532(1989).

[17] M.Honda,K.Kasahara,K.Hidaka, and S.Midorikawa, Phys.Lett.B248,193(1990).

[18] M.Honda,K.Kajita,K.Kasahara,and S.Midorikawa,
Phys.Rev.D52,4985(1995).

[19] H.Lee and Y.Koh, Nuovo Cimento B105,883(1990).

[20] E.V.Bugaev and V.A.Naumov, Phys.Lett. B232,391(1989).

[21] A.I.Alikhanyan, Proc.Moscow Cosmic Ray Conf.1,317(1959).

[22] V.V.Barmin,V.P.Kanavets, and B.V.Morozov,
Sov.Phys.JETP 12,683(1961).

[23] N.M.Kocharyan, Z.A.Kirakosyan,E.G.Sharoyan,and A.P.Pikalov,
Sov.Phys.JETP 11,12(1960).

[24] H.V.Bradt and G.N.Clark, Phys.Rev 132,1306(1963).

[25] A.I.Alikhanyan,T.L.Astiani,and E.M.Matevosyan, Sov.Phys.JETP 15,90(1962).

[26] C.S.Johnson, Phys.Rev.122,1883(1961).

[27] B.Dolgoshein,B.Luchkov, and V.Ushakov,
Sov.Phys.JETP 15,654(1962).

[28] S.N.Sen Gupta and M.S.Sinha, Proc.Phys.Soc.79,1183(1962).

[29] R.Turner,C.M.Ankenbrandt,and R.C.Larsen,
Phys.Rev.D4,17(1971).

[30] M.Yamada et al., Phys. Rev., D44, 617(1991).

[31] T.D.Lee and C.N.Yang, Phys.Rev.105,1415(1957).

[32] R.A.Mann and M.E.Rose, Phys. Rev., 121(1961) 293.

[33] T.Suzuki, D.F.Measday and J.P.Roalsvig, Phys. Rev., C35 (1987) 2212.

[34] T.Yamanaka, Doctor thesis, University of Tokyo(1984).

[35] JIS handbook 1995.

[36] Bicron Corporation, Catalog, 1994.

[37] Kraray Corporation, Catalog, 1994.

[38] Hamamatsu Photo. Co., *Photomultiplier tubes and related products*, 1994.

[39] K.Shiino, K.Kono, T.Ishii, S.Kasai, and S.Yamada,
INS-T-495, March 1990.

[40] ZEUS collaboration, The ZEUS detector, Status Report (1993).

[41] K.Nagamine and T.Yamazaki, *Muon science research at meson science laboratory, University of Tokyo (1981-1986)*, Feb.1987.

[42] Brochure of the University of Tokyo, Faculty of Science, Meson Science Laboratory, *Exploring Matter with Muons and Creating a New World*, 1994.

[43] J.I.Friedman and V.L.Telegdi, Phys.Rev.,105(1957)1681.

[44] T.Ohsuka, (private communication).

[45] W.Lohmann,R.Kopp,R.Voss, *Energy loss of muons in the energy range 1-10000 GeV*; CERN 85-03.

[46] T.Hara et al., 1979, Proc. of 16th Int. Cosmic Ray Conf. (Kyoto), 8, 135.

[47] M.Nagano, (private communication).

[48] K.Mitsui et al., Nucl. Inst. Meth. in Phys. Res. A290(1990)565.

[49] T.Aoki, (private communication).

[50] B.J.Bateman et al., Phys. Lett., 36B (1971) 144.

[51] CERN, Application Software Group, *GEANT -Detector Description and Simulation Tool*, 1993.

[52] CERN, Application Software Group, *MINUIT -Function Minimization and Error Analysis*, 1993.

[53] T.Nakano, (private communication).

[54] Proc. of the Yamada Conf. Vll, Muon Spin Rotation, Shimoda, 1983 Hyperfine Interactions 17-19 (1984) 879-884.

[55] S.Hayakawa, *Cosmic ray physics*, John Wiley and Sons, Inc., 1969.

[56] M.Honda, (private communication).

[57] T.Ishii et al., Nucl. Inst. Meth. in Phys. Res. A320(1992) 449-459.

[58] W.A.Baker et al., Phys.Rev.Lett.7,101(1961).

[59] T.Eichten et al., Nucl,Phys.B44,333(1972).

[60] K.Alpgard et al., Phys.Lett.115B,65(1982).

[61] K.Nagamine et al., Chem.Phys.Letters 87(1982)186.

[62] K.Nagamine, (private communication).

[63] T.Kajita, ICRR-Report-332-94-27.

[64] Ch.Berger *et al.*, Phys.Lett.B227,489(1989).

[65] Ch.Berger *et al.*, Phys.Lett.B245,305(1990).

[66] M.Aglietta et al., Europhys.Lett.8(1989)611.

[67] H.A.Tolhoek, Rev.Mod.Phys.28,277(1956).

[68] M.J.Berger and S.M.Seltzer, *Stopping powers and ranges of electrons and positrons*(2nd,Ed), NBSIR 82-2550-A(1982).